



**CHALMERS**  
UNIVERSITY OF TECHNOLOGY

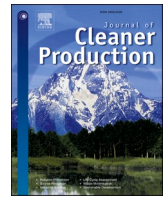
## **Reduced environmental impact of short sea shipping through optimal propulsion power allocation**

Downloaded from: <https://research.chalmers.se>, 2025-06-07 11:27 UTC

Citation for the original published paper (version of record):

Vergara, D., Lang, X., Zhang, M. et al (2025). Reduced environmental impact of short sea shipping through optimal propulsion power allocation. *Journal of Cleaner Production*, 513.  
<http://dx.doi.org/10.1016/j.jclepro.2025.145683>

N.B. When citing this work, cite the original published paper.



# Reduced environmental impact of short sea shipping through optimal propulsion power allocation

Daniel Vergara<sup>a</sup>, Xiao Lang<sup>a,\*,\*\*</sup> , Mingyang Zhang<sup>b</sup>, Martin Alexandersson<sup>c</sup>,  
Wengang Mao<sup>a,\*</sup> 

<sup>a</sup> Department of Mechanics and Maritime Sciences, Chalmers University of Technology, Gothenburg, Sweden

<sup>b</sup> Department of Mechanical Engineering, Aalto University, Espoo, Finland

<sup>c</sup> SSPA Maritime Centre, RISE, Gothenburg, Sweden

## ARTICLE INFO

### Keywords:

Ship energy efficiency  
Emission reduction  
Propulsion power allocation  
Voyage segmentation  
Dynamic programming  
Decarbonization  
Maritime transport

## ABSTRACT

To reduce the environmental impact of short sea shipping, this study introduces a two-stage propulsion power allocation method aimed at enhancing ship operational efficiency in various weather environments. The first stage utilizes a metocean score-based pruned explicit linear time (MS-PELT) algorithm to segment the trajectory into several legs based on metocean conditions, thereby minimizing frequent engine setting adjustments and simplifying the optimization process. In the second stage, a parallel coupling Dynamic Programming (PCDP) method is introduced to optimize power allocation in each leg using machine learning-based ship performance models. The proposed approach is evaluated using three years of full-scale operational data from a case study chemical tanker. Results show that the MS-PELT method outperforms the state-of-the-art multivariate clustering algorithm by providing practical and efficient segmentation. The optimized power allocation strategy demonstrates a promising average of 8 % emission and environmental impact reductions for case study short sea voyages with good computational efficiency. It is suitable for real-time applications, providing the maritime industry with tools to optimize ship engine settings, reducing emissions and environmental impact.

## Abbreviation

COA	Contract of Affreightments	LFO	Light Fuel Oil
DP	Dynamic Programming	MILP	Mixed Integer Linear Programming
ECA	Energy Control Area	PELT	Pruned Explicit Linear Time
EEM	Energy Efficiency Measure	IMO	International Maritime Organisation
ETA	Estimated Time of Arrival	TICC	Toeplitz Inverse Covariance Clustering
GHG	Greenhouse Gas	1-D	One-Dimensional
RMSE	Root Mean Square Error	MAPE	Mean Absolute Percentage Error

## Nomenclature

$\alpha_{current}$ [°]	Relative current angle	$H$	Number of parallel scenarios
$\alpha_h$ [°]	Relative wave angle	$H_s$ [m]	Significant wave height

(continued on next column)

## (continued)

$\alpha_{wind}$ [°]	Relative wind angle	$L_{pp}$ [m]	Length between perpendiculars
$\beta$	Metocean direction score	$ll$	Log likelihood
$\Delta$ [m <sup>3</sup> ]	Ship displacement	$m$	Number of waypoints in a leg
$\Delta T$	Maximum deviation time for one leg	$m_{fuel}$ [ton/h]	Fuel consumption rate
$\gamma g()$	PELT penalty factor	$MCR$ [kW]	Maximum continuous rating
$\Gamma$	Discrete power setting candidate	$MS$	Metocean score
$\iota$	Metocean intensity score	$\overline{MS}$	Ensemble metocean score
$\Lambda_{fuel}$	Fuel prediction model	$n$	Number of legs
$\Lambda_v$	Speed prediction model	$l$	Loss function
$\omega$	TICC subsequence length	$P$ [kW]	Ship propulsion power
$\Omega$	TICC temporal consistency parameter	$Q$	Number of simulated voyages
$\varphi$	PELT cost function	$RPM$	Engine speed

(continued on next page)

\* Corresponding author.

\*\* Corresponding author.

E-mail addresses: [xiao.lang@chalmers.se](mailto:xiao.lang@chalmers.se) (X. Lang), [wengang.mao@chalmers.se](mailto:wengang.mao@chalmers.se) (W. Mao).

<https://doi.org/10.1016/j.jclepro.2025.145683>

Received 25 December 2024; Received in revised form 30 April 2025; Accepted 8 May 2025

Available online 10 May 2025

0959-6526/© 2025 The Authors. Published by Elsevier Ltd. This is an open access article under the CC BY license (<http://creativecommons.org/licenses/by/4.0/>).

(continued)

$\sigma$	PELT cluster assignment set	$t$	Time
$\tau$	Change point	$T_{design}$ [m]	Design draught
$\Theta$	Toeplitz covariance matrix	$T_{mean}$ [m]	Mean draught
$a$	Number of waypoints	$T_z$ [s]	Wave period
$b$	Number of change points	$V$ [kn]	Speed over ground
$B_m$ [m]	Moulded breadth	$V_{average}$ [kn]	Average sailing speed
$C$	Constraint function	$V_{current}$ [m/s]	Sea current speed
$C_B$	Block coefficient	$V_{max}$ [kn]	Maximum sailing speed
$d$ [km]	Accumulated sailing distance	$V_{min}$ [kn]	Minimum sailing speed
$DWT$ [tons]	Deadweight	$V_{wind}$ [m/s]	Absolute wind speed
$e$	Number of discrete candidates	$\bar{w}$	Mean metocean condition
$f$ [tons]	Emission for one leg	$\mathbf{W}$	Metocean matrix
$F$ [tons]	Accumulated emission	$x$ [°]	Longitude
$G$	Decision tree in XGBoost	$y$ [°]	Latitude

## 1. Introduction

Shipping contributes to 3 % of global greenhouse gas (GHG) emissions, and this share is projected to continue rising without intervention (UNCTAD, 2023; IMO, 2020). The International Maritime Organisation (IMO) has imposed stricter regulations to reduce shipping emissions, and shipping companies are all prioritizing energy efficiency measures (EEM) to comply with regulations and reduce operational costs (IMO, 2023). It impacts all shipping stages, from initial planning to real-time decision-making at sea. For instance, shipping companies use the departure and destination ports, and the estimated time of arrival (ETA) specified by the contract of affreightment (COA) to select the optimal route and speed before the journey (Wang et al., 2021).

Despite careful planning, onboard crews often need to adjust the power settings based on actual weather conditions to meet the ETA, and reduce GHG emission/fuel consumption (Lang et al., 2024). During navigation at sea, onboard crews adjust propulsion settings less frequently compared to operations near ports, typically for several hours, depending on environmental changes, traffic, or operational needs (Wang et al., 2017, 2018; Fan et al., 2024). Automatic control mechanisms, such as autopilot, usually manage navigation, ensuring the ship maintains its set course or follows a predetermined route (Fossen, 2002). Currently, most ship operation optimization research has focused on speed as the primary control variable. However, these methods face challenges in practical application. The propulsion system indirectly controls ship speed, and maintaining a constant or piecewise set-point speed requires continuous propulsion adjustments to respond to fluctuating metocean conditions (Fan et al., 2022). Frequent adjustments to engine speed, engine power, and propeller pitch can reduce energy efficiency and accelerate component wear (Sørensen et al., 1997; Sørensen, 2013; Yu et al., 2024).

Therefore, introducing a method to efficiently segment a voyage into an optimal number of legs (characterized by relatively uniform sailing environments), and then optimizing power allocation for these segments becomes meaningful. Currently, research has seldom explored power allocation optimization combined with voyage segmentation based on real metocean conditions. Processing large volumes of metocean data can negatively impact computational performance, leading to overly segmented routes that are inefficient for practical application. This study proposes a novel power allocation optimization method for short sea shipping, which typically follows a predefined and fixed trajectory. The method addresses the one-dimensional (1-D) power allocation problem in two stages. First, the fixed route is segmented into legs using the pruned exact linear time (PELT) algorithm (Killick et al., 2012), based on an ensemble metocean score derived from metocean conditions. Next, ship performance models, built using the XGBoost algorithm, are combined with a newly developed parallel coupling Dynamic

Programming to determine the optimal power setting for each leg, minimizing GHG, more specifically, CO<sub>2</sub> emissions. This approach reduces the number of transients experienced by the propulsion system during the voyage while ensuring that the ETA is met.

The remainder of this paper is organized as follows: Section 2 reviews and discusses the related literature, Section 3 introduces the proposed framework for optimal power allocation, and Section 4 shows the full-scale measurements and details of performance modeling. Section 5 presents case studies demonstrating the effectiveness of the proposed method. Finally, Section 6 draws the conclusions.

## 2. Literature review

### 2.1. Ship operation optimization

Choosing the optimization variable is indeed fundamental to determining the optimal sailing strategy. Most existing studies chose speed as the optimization variable, since it is easier for the optimization algorithms to search for waypoints and weather conditions for candidate routes and ensure accurate arrival time. (Zheng et al., 2019; Ma et al., 2021; Jimenez et al., 2022; Luo et al., 2023; Yan et al., 2024). These research address methods for solving speed allocation optimization problems to identify optimal speed profiles that minimize fuel consumption and enhance computational efficiency. Common approaches include genetic algorithms (Wang et al., 2020; Yeh and Tan, 2021; Han et al., 2023), proxy optimization (Vergara et al., 2023; Yu et al., 2024), mixed integer linear programming (MILP) (Psarافتis and Kontovas, 2014; Fagerholt et al., 2015; Kim et al., 2019; Ma et al., 2021; Xie et al., 2023), and reinforcement learning (Shang et al., 2024).

Dynamic Programming (DP), based on Bellman's principle of optimality (Bellman, 1952), has also been extensively applied to this purpose. By discretizing the navigation process into a constructed grid, DP decomposes the global optimization problem into a series of stage-wise subproblems. Specifically, the voyage is divided into multiple time and/or spatial stages, where recursive calculations are performed to determine the optimal solutions for each subproblem and then form the optimal solution for the entire voyage. Early applications of DP for voyage optimization focused on integrating environmental data to minimize fuel costs. Calvert et al. (1991) employed isochrones to partition the route into stages, aligning weather forecasts with each segment, and then applying DP to optimize fuel consumption for transatlantic crossings. Shao et al. (2012) developed a three-dimensional DP (3DDP) for ship weather routing using fixed distance intervals along a great circle route. Kim and Lee (2018) applied DP to optimize ship speed along predetermined routes for energy efficient navigation. Zaccone et al. (2018) proposed a 3DDP algorithm to optimize ship speed profiles that segmented the route spatially along a great circle path, defining alternative states based on transverse deviation and discrete arrival times. Recent studies have focused on improving DP efficiency through optimization techniques. Du et al. (2022) employed a 3DDP algorithm for weather routing, incorporating multi-objective optimization and dynamic route updates using real-time weather forecasts. Jeong and Kim (2023) introduced a graph-based optimization approach using AIS-derived waypoints, calculating fuel costs under time-varying conditions to optimize ship route and speed by DP.

Despite these advancements, a fundamental limitation persists across these studies: the recursive nature of DP inherently reduces efficiency due to strong temporal coupling. Each stage's computation relies on the results from previous stages, enforcing a strict sequential order. This dependency significantly reduces computational efficiency, especially when real-time updates are required. The inability to decouple subproblems along the time dimension prevents parallel processing, resulting in longer computation times and reduced scalability.

Moreover, the propulsion system only indirectly controls the ship's speed. For speed-based optimization, maintaining a constant or piecewise set-point speed under fluctuating metocean conditions requires

continuous engine power adjustments, which can reduce energy efficiency and increase engine wear (Yu et al., 2024). On the other hand, speed-based optimization allows for direct estimation of sailing time and ETA, but it also requires ship performance models to predict required propulsion power and fuel consumption. An alternative approach is to directly optimize engine power, which provides a more stable engine load and is easier to implement onboard. This method requires reliable models to predict ship speed based on power and environmental conditions to meet ETA requirements (Wang et al., 2017; Wang, 2020). Regardless of the strategy, speed-based or power-based optimization, uncertainties arising from the ship performance model are inevitable.

Exploring power-based optimization as a more straightforward alternative is therefore meaningful, especially as it remains underexplored in current research. It offers a more straightforward and practical solution for onboard implementation and mitigates inefficiencies by minimizing the need for frequent adjustments through proper voyage segmentation. Recent advances in machine learning and big data analytics have helped address performance modeling challenges, enabling more accurate ETA predictions and more energy-efficient engine power settings (Yan et al., 2020; Laurie et al., 2021; Lang et al., 2022; Zhang et al., 2024; Shu et al., 2024). Methods developed for speed allocation optimization can also be adapted for power allocation. For instance, DP has proven effective in identifying optimal ship speed discrete set-points to meet ETA constraints while minimizing fuel consumption (Wang et al., 2018). A common limitation of many speed optimization approaches is the assumption of static metocean conditions for computational simplicity. In reality, dynamic conditions often require frequent speed adjustments, slowing in harsh weather and accelerating in calm seas (Li et al., 2020, 2023; Wei et al., 2022). In contrast, power-based optimization aims to minimize such adjustments, and determining an optimal number of voyage segments is essential to balance performance and accuracy.

## 2.2. Voyage segmentation

For liner shipping networks with speed adjustments, each route segment is defined as the trajectory between two ports (Wang et al., 2019; Qi and Song, 2012; Guericke and Tierney, 2015; Wang et al., 2018; Wu, 2020; Sung et al., 2022). Over time, different methods have been proposed for segmenting a fixed route, and the most common approaches are summarized in Fig. 1.

When allocating speed for different legs within a voyage, most existing methods divide the route into segments with equal distance or time based on grids or waypoints (Tzortzis and Sakalis, 2021; Wang et al., 2021; Lee et al., 2023). With the advent of digitalization and big data analytics in shipping, newer approaches use clustering algorithms applied to time series data to identify different operational patterns. A widely used technique for segmenting routes and extracting route structures from data is the turning point method. Zhang et al. (2018) and He et al. (2019) utilized turning points to identify route segments and detect potential collision points, while Wen et al. (2019) combined turning points with DBSCAN clustering on historical route data to define segments. Zhang et al. (2021) linked sequences of turning point regions to delineate complete routes, and Yan et al. (2020) utilized turning points to define critical waypoints along a route. Integrating this approach with optimization, Li et al. (2022, 2023) employed turning points to achieve trajectory segmentation and minimize fuel consumption, and Zhang et al. (2024) similarly used turning points to divide routes into effective legs. However, these approaches often overlook the impact of metocean conditions on ship performance, even though metocean conditions vary significantly during a single voyage. Despite the extensive literature on speed optimization and a variety of segmentation methods, the sequential integration of route segmentation and power allocation optimization remains underexplored.

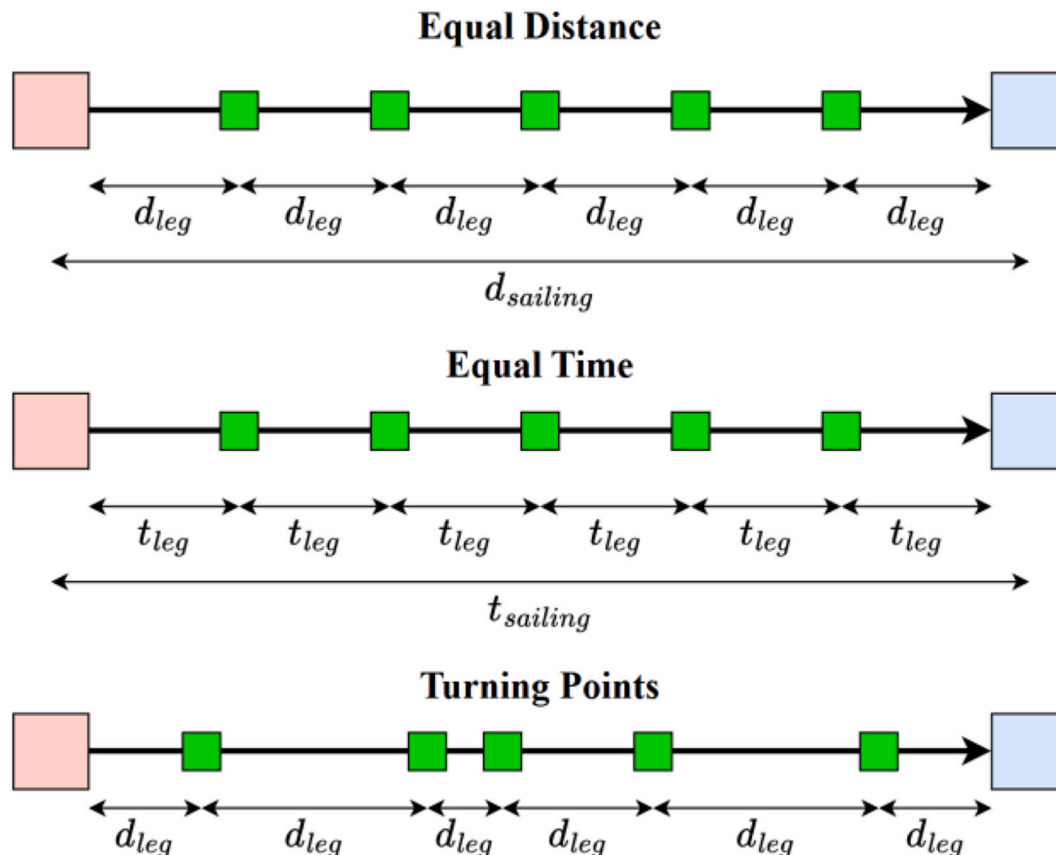


Fig. 1. Common segmentation approach used in the voyage optimization literature.

### 2.3. Contribution of this study

To sum up, most existing ship operation optimization methods focus on speed-based strategies, which require continuous propulsion adjustments under dynamic metocean conditions, and may lead to reduced energy efficiency and operational complexity. Existing segmentation techniques also tend to oversimplify route partitioning by ignoring environmental variability, and traditional DP methods suffer from computation efficiency due to their sequential nature and inability to parallelize across time stages.

To bridge these gaps, we propose a novel two-stage framework for ship power allocation in short-sea shipping that combines metocean-based voyage segmentation with a parallel coupled DP method. The key contributions are as follows:

- Introduce a data-driven voyage segmentation method based on an ensemble metocean score derived from encountered environmental conditions (e.g., wind, wave, and current). This approach segments the voyage into spatially and temporally contiguous legs with homogeneous metocean conditions, addressing the limitations of traditional equal-distance/time or turning-point methods that overlook environmental variability.
- Propose a more practical and straightforward power-based optimization strategy that directly allocates ship propulsion power instead of ship speed. This method reduces the need for frequent engine adjustments in dynamic conditions, offering a stable engine load and simpler onboard implementation.
- Develop a parallel coupled DP algorithm that integrates pre-simulated sailing scenarios and links route segments through predefined arrival time ranges. This design improves computational efficiency, enabling partial parallelization of the optimization process while accounting for metocean uncertainties. The method supports near-real-time decision making and enhances scalability.

The proposed framework is validated using full-scale operational data from a short-sea chemical tanker. Results demonstrate reduced emissions, confirming the practical value of the method for ship operation optimization in real world.

### 3. Methodology

#### 3.1. Workflow of the proposed propulsion power allocation method for short sea shipping

Short sea shipping involves transporting cargo and passengers by sea without crossing an ocean, using ports and inland waterways to complement traditional cargo transport methods (Papadimitriou et al., 2019). This mode of transport offers an alternative to road and rail, aiming to alleviate congestion, reduce emissions, and lower transportation costs. Fig. 2 illustrates the 166 routes of a case study chemical tanker over three years within Europe.

It is clear that short sea shipping often follows consistent trajectories between the same departure and destination ports, with considerable overlap among different voyages. This consistency can be attributed, in part, to the relatively moderate wave conditions typically encountered in short sea shipping, as compared to transoceanic voyages. These conditions reduce the need for voyage alterations to avoid severe weather, enabling vessels to adhere to predefined sailing trajectories in accordance with the emission control area (ECA).

Given that the sailing trajectory for short sea shipping is typically predefined, propulsion power allocation is assumed to be a 1-D optimization problem along a fixed route in this study. The detailed framework of the proposed two-stage power allocation optimization method for short sea shipping is illustrated in Fig. 3. This method addresses the allocation in two stages:

- **Stage I: Voyage segmentation.** In this stage, the predefined fixed route is divided into several legs using a metocean based segmentation algorithm to minimize frequent adjustments to the power setting. The trajectory (longitude and latitude) and ETA (determines the timestamps for each waypoint) are used to match wind, wave, and current data encountered along the route. Segmentation is then performed based on a novel ensemble metocean score, which accounts for the overall environmental variability. The output of this stage is a set of voyage legs, each characterized by relatively consistent metocean conditions. These segments serve as the input for the stage II, ensuring a natural transition and reducing the complexity of the subsequent optimization task.

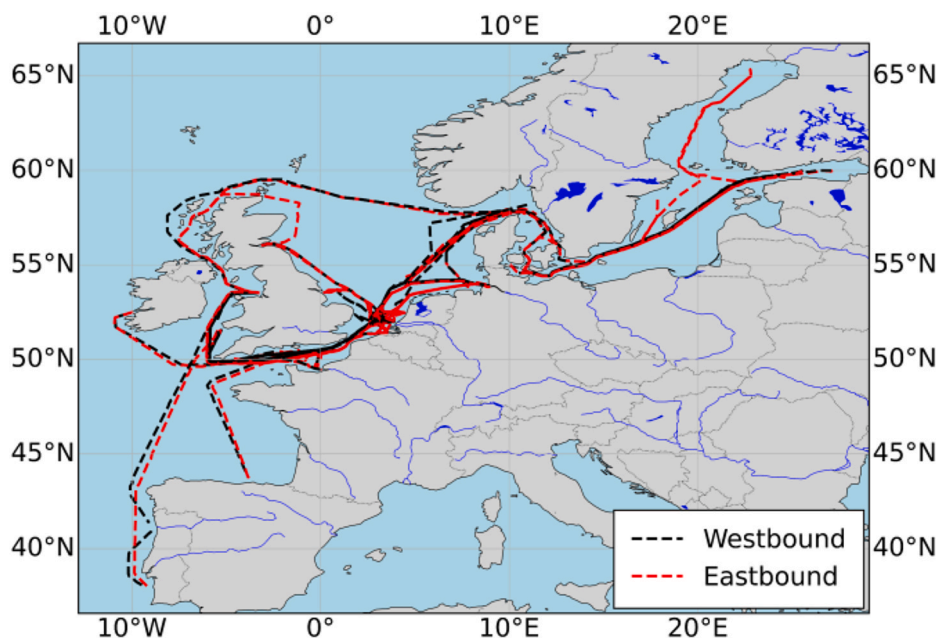


Fig. 2. Typical trajectories of a case study chemical tanker over three years sailing.

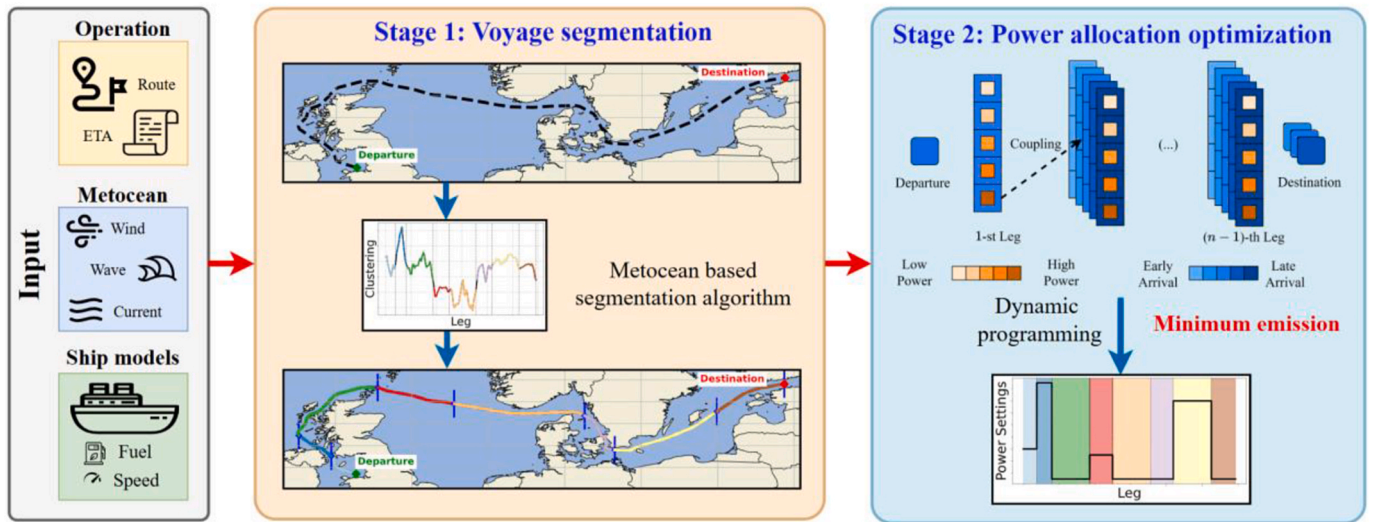


Fig. 3. The proposed two-stage propulsion power allocation optimization framework for short sea shipping.

• **Stage II: Power allocation optimization.** Using the segmented legs generated in Stage I, the optimal power allocation for each leg is determined via a newly proposed parallel coupling DP algorithm. Ship speed and fuel consumption are evaluated through machine learning models. Multiple parallel sailing scenarios are pre-simulated and stored, with each leg interconnected by defined arrival time ranges to help mitigate uncertainties in metocean conditions. These pre-simulations enable fast and efficient propulsion power allocation optimization across the entire voyage, aiming to reduce CO<sub>2</sub> emissions.

In the following subsections, the proposed voyage segmentation method is detailed in Section 3.2, followed by the parallel coupling DP approach for power allocation optimization in Section 3.3.

### 3.2. Voyage segmentation

This study proposes a voyage segmentation method, namely metocean score-based Pruned Exact Linear Time (MS-PELT) algorithm, to provide the optimal number of legs. To evaluate its effectiveness and efficiency, the proposed method is compared to a well-known multivariate time series clustering algorithm known as Toeplitz inverse covariance-based clustering (TICC).

#### 3.2.1. MS-PELT algorithm

The proposed MS-PELT algorithm consists of four steps, as illustrated in Fig. 4. In step 1, the average speed  $V_{average}$  required to meet the ETA

based on the total distance  $D$  of the predefined trajectory is determined. Next, Monte Carlo simulations are applied to generate a series of reference voyages. These voyages feature different speed profiles, but all maintain an average speed  $V_{average}$  within a sailing speed range constrained by  $[V_{min}, V_{max}]$ . These randomized reference voyages help estimate the metocean conditions the ship will likely encounter at each waypoint along the route. In step 2, the corresponding metocean conditions for each waypoint (timestamps updated based on Monte Carlo simulated speed) are extracted across each reference voyage. Step 3 calculates a metocean score for each waypoint, representing the aggregated impact of various metocean factors. This score results in an ensemble metocean signal that integrates the variability of all metocean variables across all reference voyages. Finally, step 4 applies the PELT algorithm to this ensemble signal to detect change points, thus segmenting the route into optimal legs. These segments are designed to minimize metocean variability within each leg, thereby supporting power allocation decisions.

During the Monte Carlo generation of reference voyages, the voyage is not yet divided into legs. The waypoints are predetermined based on their locations (longitudes  $x$  and latitudes  $y$ ), spaced at equal intervals corresponding to approximately 1 h of sailing at the average speed  $V_{average}$ . The metocean score for each waypoint consists of two components: a direction score ( $\beta$ ), associated with the relative angle of metocean variables (wind, wave, current), and an intensity score ( $\nu$ ), related to the magnitude of the metocean variables. The considered metocean variables at and  $k$ -th waypoint on the  $q$ -th reference voyage are denoted as

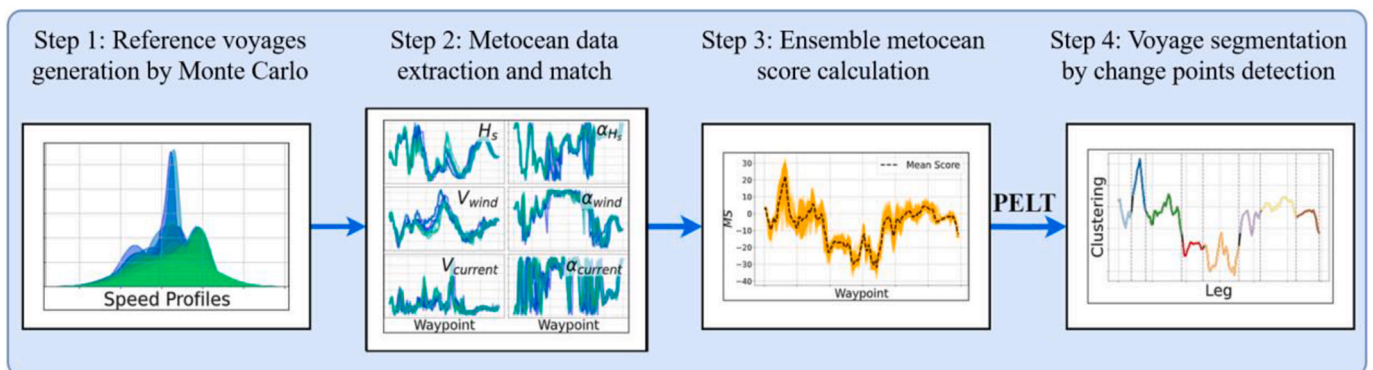


Fig. 4. The workflow of the proposed MS-PELT voyage segmentation method.

$$\mathbf{MO}_{q,k} = \left[ H_s(q,k), \alpha_{H_s}(q,k), V_{wind}(q,k), \alpha_{wind}(q,k), V_{current}(q,k), \alpha_{current}(q,k) \right], \quad (1)$$

where  $H_s$  is the significant wave height,  $\alpha_{H_s}$  is the relative wave angle,  $V_{wind}$  is the absolute wind speed,  $\alpha_{wind}$  is the relative wind angle,  $V_{current}$  is the absolute current speed, and  $\alpha_{current}$  is the relative current angle. All these values are determined using trilinear interpolation (location and time) of hindcast data. The direction score  $\beta$  classifies the favourability of metocean direction on a scale ranging from  $-5$  to  $+5$  for every  $30^\circ$  interval, as shown in Table 1.

The intensity score  $i$  is determined using well-established scales, such as the Beaufort scale for wind speed and the Douglas sea scale for significant wave height. For sea current, a simple numerical scale ranging from 0 to 10 is used, as presented in Table 2.

For the  $k$ -th waypoint on the  $q$ -th reference voyage, the metocean score  $MS_{q,k}$  is calculated as

$$MS_{q,k} = \beta \left[ \alpha_{H_s(q,k)} i [H_s(q,k)] + \beta \left[ \alpha_{wind(q,k)} i [V_{wind}(q,k)] + \beta \left[ \alpha_{current(q,k)} i [V_{current}(q,k)] \right] \right] \right] \quad (2)$$

The final ensemble metocean score for the  $k$ -th waypoint,  $\overline{MS}_k$ , is obtained by averaging the metocean scores across all  $Q$  reference voyages as

$$\overline{MS}_k = \frac{1}{Q} \sum_{q=1}^Q MS_{q,k}. \quad (3)$$

Given the obtained 1-D series data of ensemble metocean score of all waypoints along the route,  $\overline{MS}_{1:a} = (\overline{MS}_1, \overline{MS}_2, \dots, \overline{MS}_a)$ , where  $a$  is the total number of the waypoints. The series data are split into  $b+1$  segments with  $b$  change points (not including the first and last point) at positions  $\tau = (\tau_1, \tau_2, \dots, \tau_b)$ .  $\tau_j$  is integer, and  $0 = \tau_0 < \tau_1 < \tau_2 < \dots < \tau_b < \tau_{b+1} = a$ . The  $j$ -th segment is denoted as  $\overline{MS}_{(\tau_{j-1}+1):\tau_j}$ . The multiple change points detection is formulated as an optimization problem finding a feasible sequence segmentation  $\tau$  that minimizes the function given by

$$\tau = \underset{\tau}{\operatorname{argmin}} \left( \sum_{j=1}^{b+1} \varphi \left( \overline{MS}_{(\tau_{j-1}+1):\tau_j} \right) + \gamma \cdot g(b) \right), \quad (4)$$

where  $\varphi$  is the cost function for each segment, and  $\gamma \cdot g(b)$  is a penalty factor that considers the complexity of the segmentation against overfitting. The cost function  $\varphi$  is defined as the  $L_2$ -norm in this study expressed by

$$\varphi \left( \overline{MS}_{(\tau_{j-1}+1):\tau_j} \right) = \sum_{i=\tau_{j-1}+1}^{\tau_j} \left( \overline{MS}_i - u \left( \overline{MS}_{(\tau_{j-1}+1):\tau_j} \right) \right)^2, \quad (5)$$

where  $u \left( \overline{MS}_{(\tau_{j-1}+1):\tau_j} \right)$  represents the mean value of the  $j$ -th segment sequence  $\overline{MS}_{(\tau_{j-1}+1):\tau_j}$ . This study employs the PELT algorithm to minimize Eq. (4), which utilizes DP to search for optimal change points,

**Table 1**  
The direction score  $\beta$  assigned to different metocean direction intervals.

Metocean direction ( $^\circ$ )	$\beta_i$
165-180	-5
135-165	-3
105-135	-1
75-105	0
45-75	1
15-45	3
0-15	5

balancing computational cost and accuracy. A key assumption is that the penalty factor is linear with the number of change points, i.e.,  $g(b) = b$ . Substituting Eq. (5) into Eq. (4), we have the objective function for the voyage segmentation given by

$$\tau = \underset{\tau}{\operatorname{argmin}} \left\{ \sum_{j=1}^{b+1} \sum_{i=\tau_{j-1}+1}^{\tau_j} \left( \overline{MS}_i - u \left( \overline{MS}_{(\tau_{j-1}+1):\tau_j} \right) \right)^2 + \gamma \cdot b \right\}. \quad (6)$$

The PELT algorithm is designed to find a balance between accurately fitting data and maintaining segmentation that is not excessively complex. This equilibrium is achieved by identifying a set of change points  $\tau$  (both in quantity and location) that minimize Eq. (6). Its pruning technique is a distinctive feature of the PELT algorithm. More details can be found in Killick et al. (2012). During the computational process, it discards specific candidate change points, effectively reducing the number of potential segments that require evaluation. Finally, the total number of legs  $n = b + 1$  is obtained through the PELT algorithm. The implementation of voyage segmentation using the proposed metocean score-based PELT algorithm is provided in Appendix Table A1 for reference.

### 3.2.2. TICC algorithm

The TICC algorithm, proposed by Hallac et al. (2017), is a well-established method for clustering multivariate time series and identifying repeating patterns in time-series data. Compared to the proposed MS-PELT algorithm, TICC uses a different input format, specifically, the average of metocean conditions across all reference voyages for each waypoint, rather than the ensembled metocean score, as a  $6 \times a$  matrix by

$$\overline{\mathbf{w}} = \begin{bmatrix} \overline{H}_s(1) & \overline{H}_s(2) & \dots & \overline{H}_s(a) \\ \overline{\alpha}_{H_s(1)} & \overline{\alpha}_{H_s(2)} & \dots & \overline{\alpha}_{H_s(a)} \\ \vdots & \vdots & \ddots & \vdots \\ \overline{\alpha}_{current(1)} & \overline{\alpha}_{current(2)} & \dots & \overline{\alpha}_{current(a)} \end{bmatrix}, \quad (7)$$

where  $a$  is the total number of the waypoints. Then the original series data are divided into short subsequences of fixed length  $\omega$  to facilitate the analysis of correlations between them. The subsequence at  $k$ -th waypoint is represented as a  $6 \times \omega$  vector by

$$\overline{\mathbf{w}}_k = \begin{bmatrix} \overline{H}_s(k-\omega+1) & \overline{H}_s(k-\omega+2) & \dots & \overline{H}_s(k) \\ \overline{\alpha}_{H_s(k-\omega+1)} & \overline{\alpha}_{H_s(k-\omega+2)} & \dots & \overline{\alpha}_{H_s(k)} \\ \vdots & \vdots & \ddots & \vdots \\ \overline{\alpha}_{current(k-\omega+1)} & \overline{\alpha}_{current(k-\omega+2)} & \dots & \overline{\alpha}_{current(k)} \end{bmatrix}. \quad (8)$$

As such, rather than clustering the individual waypoints directly, TICC instead consists of clustering these subsequences  $\{\overline{\mathbf{w}}_1, \overline{\mathbf{w}}_2, \dots, \overline{\mathbf{w}}_a\}$ . In TICC, each cluster is defined by a Gaussian inverse covariance  $\theta_j$ , and it defines a Markov random field (MRF) encoding the structural representation of the  $j$ -th cluster. The objective is to solve these  $n$  inverse covariances  $\theta = \{\theta_1, \dots, \theta_n\}$ , one per cluster, and the resulting assignment sets  $\sigma = \{\sigma_1, \dots, \sigma_n\}$ , where  $\sigma_i \subset \{1, 2, \dots, a\}$ . The overall optimization problem is defined as

$$\theta, \sigma = \underset{\theta, \sigma}{\operatorname{argmin}} \sum_{j=1}^n \left[ \overbrace{\|\lambda \circ \theta_j\|_1}^{\text{sparsity}} + \sum_{\overline{\mathbf{w}}_k \in \sigma_j} \left( \overbrace{-\ln(\overline{\mathbf{w}}_k, \theta_j)}^{\text{log likelihood}} + \overbrace{\Omega \mathbf{1}\{\overline{\mathbf{w}}_{k-1} \notin \sigma_j\}}^{\text{temporal consistency}} \right) \right], \quad (9)$$

where  $\|\lambda \circ \theta_j\|_1$  is an  $L_1$ -norm penalty,  $\ln(\overline{\mathbf{w}}_k, \theta_j)$  is the log likelihood that  $\overline{\mathbf{w}}_k$  came from the  $j$ -th cluster, and  $\Omega$  is a parameter that enforces temporal consistency, and  $\mathbf{1}\{\overline{\mathbf{w}}_{k-1} \notin \sigma_j\}$  is an indicator function checking whether neighbouring points are assigned to the same cluster.

### 3.3. Power allocation optimization

After voyage segmentation, a voyage can be mathematically repre-

**Table 2**  
The intensity score  $i$  assigned to different ranges of wind speed, significant wave height, and current speed.

$V_{wind}$ (m/s)	0-0.2	0.2-1.5	1.5-3.3	3.3-5.4	5.4-7.9	7.9-10.7	10.7-13.8	13.8-17.1	17.1-20.7	20.7-24.4	24.4-28.4	28.4-32.6	32.6+
Beaufort scale ( $u_{wind}$ )	0	1	2	3	4	5	6	7	8	9	10	11	12
$H_s$ (m)	0-0.1	0.1-0.5	0.5-1.25	1.25-2.5	2.5-4	4-6	6-9	9-14	14+				
Douglas scale ( $H_s$ )	0	1	2	3	4	5	6	7	8				
$V_{current}$ (m/s)	0-0.1	0.1-0.2	0.2-0.5	0.5-1	1-1.5	1.5+							
Current scale ( $u_{current}$ )	0	2	4	6	8	10							

sented as a sequence of legs, power settings, and encountered metocean conditions. The waypoint vector  $\mathbf{S}$  is represented as

$$\mathbf{S}_{j,k} = [x_{j,k}, y_{j,k}, t_{j,k}], \quad (10)$$

where  $x_{j,k}$ ,  $y_{j,k}$ , and  $t_{j,k}$  denote the longitude, latitude, and timestamp, respectively, for the  $k$ -th waypoint within the  $j$ -th leg, as Fig. 5 shows.

The power setting  $\mathbf{P}$  represents the propulsion power allocation for each leg of the route, expressed as

$$\mathbf{P} = [P_1, \dots, P_j, \dots, P_n], \quad (11)$$

where  $n$  is the total number of legs in the route obtained by voyage segmentation. For each leg, the power setting is assumed to be constant. The metocean matrix  $\mathbf{W}$  represents the encountered metocean conditions at each waypoint along the route, defined as

$$\mathbf{W} = \begin{bmatrix} [\mathbf{W}_{1,1}, \dots, \mathbf{W}_{1,m_1}] \\ \vdots \\ [\mathbf{W}_{j,1}, \dots, \mathbf{W}_{j,m_j}] \\ \vdots \\ [\mathbf{W}_{n,1}, \dots, \mathbf{W}_{n,m_n}] \end{bmatrix}, \quad (12)$$

where  $m_j$  denotes the total number of waypoints in the  $j$ -th leg, and the metocean condition at waypoint  $\mathbf{S}_{j,k}$  is defined by

$$\mathbf{W}_{j,k} = [H_{z(j,k)}, \alpha_{H_s(j,k)}, T_{z(j,k)}, V_{wind(j,k)}, \alpha_{wind(j,k)}, V_{current(j,k)}, \alpha_{current(j,k)}], \quad (13)$$

where the wave period  $T_z$ , is included in the power allocation optimization for ship speed and fuel consumption modeling. To optimize power allocation for each segment and minimize total CO<sub>2</sub> emission, the cost function representing the emission for the  $j$ -th leg is denoted as  $f_j(P_j, \mathbf{W}_{1,1 \rightarrow m_j})$ , and is defined as

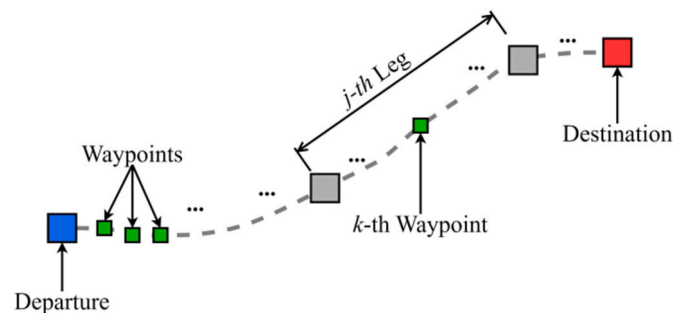


**Fig. 5.** Illustration of a route, including the  $k$ -th waypoint within the  $j$ -th leg, showing the division of the voyage into smaller navigational segments.

$$f_j(P_j, \mathbf{W}_{j,1 \rightarrow m_j}) = \sum_{k=1}^{m_j-1} r_{co_2} \cdot m_{fuel}(P_j, \mathbf{W}_{j,k}) t_{j,k \rightarrow k+1}, \quad (14)$$

where  $r_{co_2}$  denotes the emission factor,  $m_{fuel}(P_j, \mathbf{W}_{j,k})$  represents the fuel consumption rate at the  $k$ -th waypoint within the  $j$ -th leg,  $t_{j,k \rightarrow k+1}$ , is the sailing time between  $(k + 1)$ -th and  $k$ -th waypoints. Additionally, the optimization is subject to a set of constraints  $C(\mathbf{P}, \mathbf{W})$ , which considers arrival punctuality and operational limits as

$$C(\mathbf{P}, \mathbf{W}) = \begin{cases} P_{\min} \leq P_j \leq P_{\max}, \\ V_{\min} \leq V(P_j, \mathbf{W}_{j,k}) \leq V_{\max}, \\ \left| 1 - \frac{\sum_{j=1}^n \sum_{k=1}^{m_j-1} t_{j,k \rightarrow k+1}}{ETA} \right| \cdot 100\% \leq 1\%. \end{cases} \quad (15)$$

Here, the constraints  $C(\mathbf{P}, \mathbf{W})$  ensure that the power setting  $P_j$  at each leg, and ship speed  $V(P_j, \mathbf{W}_{j,k})$  at any waypoint are kept within operational limits. In this study, a 1 % deviation of the original ETA was selected based on practical considerations to accommodate sailing time constraints. The sailing times of different voyages for the case study vessels range from 100 to 150 h. Communication with ship operators indicated that a deviation of approximately 1–2 h is generally acceptable. A 1 % deviation corresponds to 1–1.5 h, aligning well with operational expectations. If the constraint margin is larger, it would be extremely difficult (sometimes impossible) for the optimization algorithm to find an optimal route with exact ETA due to uncertainties in various models. The optimization algorithm requires some flexibility during the search process to discretize the sailing area and time along the voyage. If the search space is too large, such as allowing a 5–10 % deviation, the voyage planning would effectively become a slow steaming problem, that is, the voyage planning would no longer align with the operators' expectations for a predefined ETA.

For connecting consecutive legs, a traditional method is exact coupling, as illustrated in Fig. 6. The last waypoint of the  $(j - 1)$ -th leg coincides with the first waypoint of the  $j$ -th leg, expressed as

$$\mathbf{S}_{j-1, m_{j-1}} = [x_{j-1, m_{j-1}}, y_{j-1, m_{j-1}}, t_{j-1, m_{j-1}}] = \mathbf{S}_{j, 1} = [x_{j, 1}, y_{j, 1}, t_{j, 1}]. \quad (16)$$

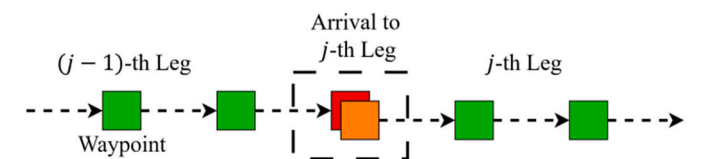


**Fig. 6.** Exact coupling between consecutive legs, where the last waypoint of  $(j - 1)$ -th leg coincides with the first waypoint of the  $j$ -th leg.

However, this approach requires sequential computation of each leg, where the starting time of each leg must be determined by the ending time of the previous one. Therefore, this method is computationally inefficient and impractical for voyages with many waypoints, as it cannot be parallelized. Therefore, this study proposes a parallel coupling DP algorithm to optimize power allocation and minimize CO<sub>2</sub> emission, as illustrated in Fig. 7.

First, a constant speed simulation determines each segment's predefined nominal departure time. For example, the nominal departure time  $t_{j,1}^{(0)}$  for the  $j$ -th leg is calculated as follows

$$t_{j,1}^{(0)} = \frac{d_{1 \rightarrow j-1}}{V_{\text{average}}}, \quad (17)$$

where  $d_{1 \rightarrow j-1}$  represents the accumulated sailing distance from the departure to the end of the  $(j-1)$ -th leg. In these parallel scenarios, the ending time of the previous segment only needs to fall within a specific time interval, defined as

$$t_{j-1,m_{j-1}} \in \left[ t_{j,1}^{(0)} - \frac{\Delta T_j}{2}, t_{j,1}^{(0)} + \frac{\Delta T_j}{2} \right]. \quad (18)$$

Suppose there are  $H$  parallel scenarios, the starting time candidates of the  $j$ -th leg can be defined by

$$t_{j,1}^{(h)} = t_{j,1}^{(0)} + h \cdot \Delta t_j, h \in \left[ 0, \pm 1, \pm 2, \dots, \pm \left\lfloor \frac{H}{2} \right\rfloor \right], \quad (19)$$

where  $\Delta t_j = \frac{\Delta T_j}{H-1}$ , and  $\Delta T_j$  is the max deviation time for the  $j$ -th leg, given by,

$$\Delta T_j = \max \left( 10 \text{ minutes}, \left\lceil 0.25 \cdot t_{j,1}^{(0)} \right\rceil \right). \quad (20)$$

For each starting candidate, simulations are conducted with different power settings for that leg. Assume the power setting is selected from a discrete set, denoted from low to high as  $[\Gamma_1, \Gamma_2, \dots, \Gamma_e]$ , where there are  $e$  possible values. In all simulations, only the scenarios where the arrival time is within the specific time interval defined by Eq. (18) are considered valid. For all legs (except the first and the last), each starting candidate for the leg is paired with all power setting from  $[\Gamma_1, \Gamma_2, \dots, \Gamma_e]$  to simulate  $e$  possible sub-voyages, which are eventually connected to the destination within the ETA tolerance, as Fig. 8 shows.

From all these parallel scenarios, the optimal power allocation for all

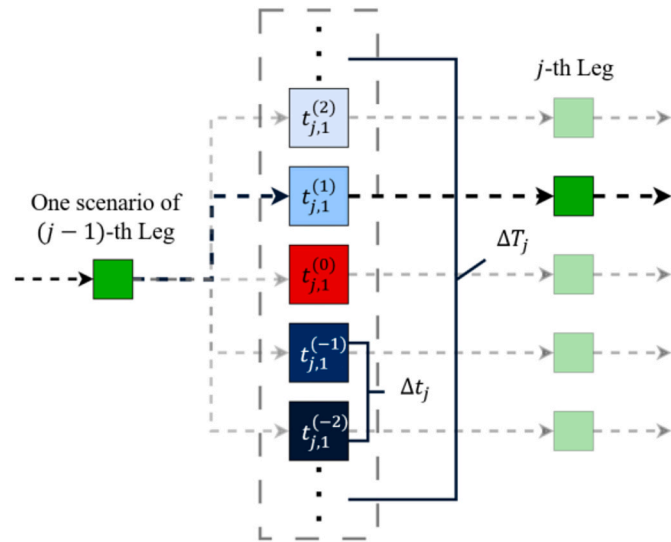


Fig. 7. Parallel coupling between consecutive legs, where the last waypoint of  $(j-1)$ -th leg (with power setting  $P_{j-1}$ ) is connected to the starting candidate of the  $j$ -th leg based on a closest time.

legs is determined to minimize the total CO<sub>2</sub> emission of the entire voyage, which is achieved using DP. Specifically, the problem can be written in the form of the Bellman's equation as

$$F_j = \min_{P_j} \left\{ f_j(P_j, \mathbf{W}_{j,1 \rightarrow m_j}) + F_{j-1} \right\}, \quad (21)$$

where  $F_j$  is the accumulated CO<sub>2</sub> emission until the end of the  $j$ -th leg.  $f_j(P_j, \mathbf{W}_{j,1 \rightarrow m_j})$  denotes the emission for the  $j$ -th leg, where  $P_j \in [\Gamma_1, \Gamma_2, \dots, \Gamma_e]$ . The DP approach iteratively solves for the minimum CO<sub>2</sub> emission, leveraging the recursive relationship between subsequent legs. The implementation of propulsion power allocation optimization using the proposed parallel coupling DP is provided in Appendix Table A2 for reference.

#### 4. Case study and details of performance modeling

This section introduces the case study ship, along with its full-scale measurements. The data processing steps and the development of ship performance models using XGBoost machine learning techniques are also briefly presented.

##### 4.1. Data acquisition

The case study ship is a chemical tanker operating in European waters, with three years of operational data available from November 2020 to March 2024. The sailing regions include the Baltic Sea, North Sea, English Channel. The three-year sailing trajectories are illustrated in Fig. 1, and the main characteristics of the chemical tanker are provided in Table 3.

The case study vessel's main engine is a MAN B&W Diesel AG - Augsburg 1 x 6L48/60B, with an MCR of 7200 kW. According to information provided by the shipowner, one of the auxiliary generators is driven by the main engine through the shaft generator system and consumes 1875 kW under a constant power take off regime. Therefore, normally, the maximum ship propulsion power for this ship is 5325 kW. In the full-scale measurement used in this study, the ship propulsion power was measured by a shaft power meter system. The raw measurements were recorded at a frequency of 1 min and subsequently down-sampled to 10-min mean values for the case study ship.

The full-scale measurements influenced by voluntary acceleration, deceleration, and transient conditions were filtered out using the 3-sigma (rolling standard deviation) method on ship propulsion power  $P$  and ship speed  $V$ . Fig. 9 presents a one-month example showing the raw measurements and processed data after 3-sigma filtering for ship speed  $V$ . The spike values and transient fluctuations caused by acceleration and deceleration have been effectively removed, leaving only relatively stable variations in the ship's operational profile.

The distribution comparison between the raw and processed data for fuel consumption rate, propulsion power, and RPM is presented in Fig. 10. It is evident that the 3-sigma filtering process effectively removed many low RPM data typically associated with transient, such as acceleration. As a result, the processed data predominantly reflects normal sailing conditions, with RPM values concentrated around 400 or 500. This filtering ensures that only stable operating conditions are retained for subsequent modeling and analysis, improving the reliability of the data-driven performance evaluation.

The metocean data, including wind and waves, were extracted from the ERA5 reanalysis dataset, which provides hourly data at a  $5^\circ \times 5^\circ$  spatial resolution (Copernicus, 2020). Ocean current velocity and direction were obtained from the Global Ocean Physics Analysis and Forecast dataset (CMEMS, 2023), with a geographical resolution of  $0.083^\circ \times 0.083^\circ$  and a temporal resolution of 30 min. The required relative wave angles, i.e.,  $\alpha_{H_s}$ ,  $\alpha_{\text{wind}}$ , and  $\alpha_{\text{current}}$ , were then calculated using the extracted metocean data and ship operation data.

The proposed power allocation optimization requires a discrete set

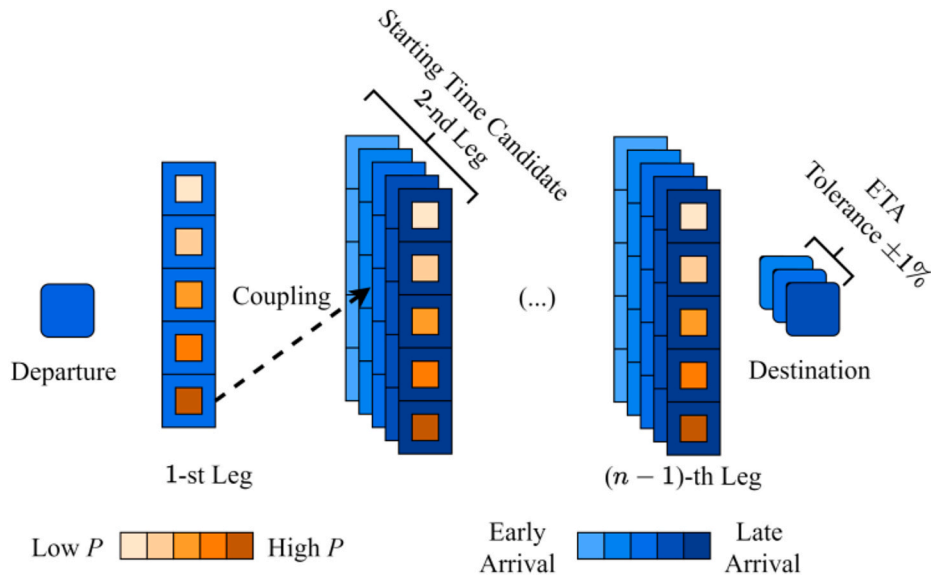


Fig. 8. Illustration of parallel coupling for optimizing power allocation across voyage legs.

Table 3

Main characteristics of the case study chemical tanker.

Parameter	Symbol	Unit	Value
Length Between Perpendiculars	$L_{pp}$	m	138.22
Breadth Moulded	$B_m$	m	23.76
Design draft	$T_{design}$	m	9.27
Block Coefficient	$C_B$	–	0.827
Displacement	$\Delta$	tons	25174
Deadweight	$DWT$	tons	18561
Maximum continuous rating (main engine)	$MCR$	kW	7200
Power Take Off from main engine (power of shaft generator)	$PTO$	kW	1875
Service speed	$V_s$	knots	14

$[\Gamma_1, \Gamma_2, \dots, \Gamma_e]$ , from which the power setting for each leg must be chosen. In this study, the discrete set is determined based on the statistics of the measured ship propulsion power  $P$  over the 3-year sailing period, as presented in Fig. 11. The ship's propulsion power primarily ranges from 1000 kW to 4300 kW, with the majority of data concentrated between 2000 kW and 3000 kW. Therefore, the bounds of the discrete set for the power setting candidates are defined with a lower bound of 1000 kW and an upper bound of 4300 kW, with increments of 100 kW, and  $[\Gamma_1, \Gamma_2, \dots, \Gamma_e] = [1000 \text{ kW}, 1100 \text{ kW}, \dots, 4300 \text{ kW}]$ , to ensure the power allocation

feasibility.

#### 4.2. Data-driven ship performance modeling

The machine learning model to predict ship speed  $V$  and fuel consumption rate  $m_{fuel}$  at each waypoint, under different power settings and metocean conditions, are established using XGBoost regression models in this study, due to its superior performance and efficiency in ship speed-power modeling (Lang et al., 2022). XGBoost is a machine learning technique designed to construct an ensemble of regression trees using a procedure known as gradient tree boosting. Its main objective is to link a set of input features, denoted by  $\bar{\mathbf{X}}$ , to a target measure. In this study, the target values are the ship's speed  $V$  and the fuel consumption rate  $m_{fuel}$ . The input features of the XGBoost model for predicting ship speed,  $\Lambda_V$ , and for predicting fuel consumption,  $\Lambda_{fuel}$ , are defined as follows

$$\bar{\mathbf{X}}_V = [P, RPM, T_{mean}, H_s, \alpha_{H_s}, T_z, V_{wind}, \alpha_{wind}, V_{current}, \alpha_{current}], \quad (22)$$

$$\bar{\mathbf{X}}_{fuel} = [P, V, RPM, T_{mean}, H_s, \alpha_{H_s}, T_z, V_{wind}, \alpha_{wind}, V_{current}, \alpha_{current}], \quad (23)$$

where  $RPM$  is the engine speed, and  $T_{mean}$  represents the ship's mean draft. Assume that the XGBoost model comprises a total of  $U$  decision

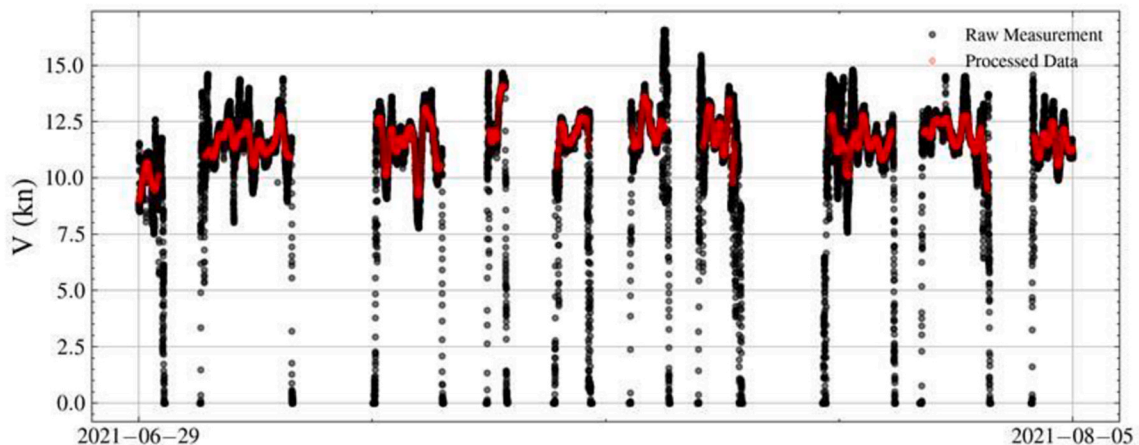


Fig. 9. Raw and processed ship speed data after 3-sigma filtering over a one-month period.

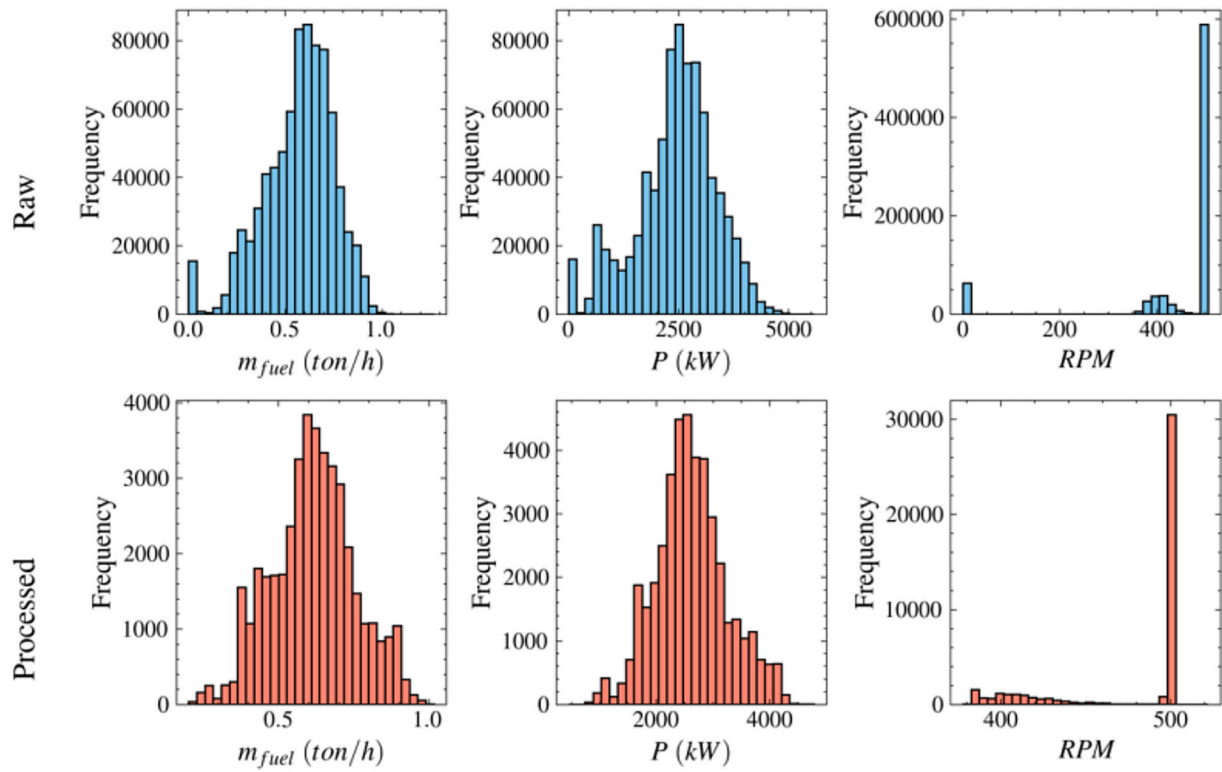


Fig. 10. Distribution comparison of raw and processed data for fuel consumption rate (left), propulsion power (middle), and RPM (right).

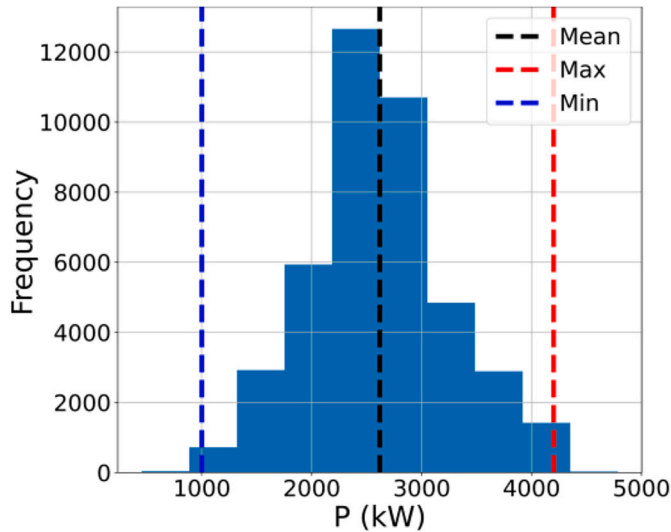


Fig. 11. Distribution of measured ship propulsion power  $P$  over the 3-year sailing period, showing the mean, maximum, and minimum power levels.

trees. For the  $i$ -th sample, the predicted speed  $\hat{V}$  is given by

$$\hat{V}_i = \sum_{u=1}^U G_u(\bar{\mathbf{X}}_{V_i}), i = 1, 2, \dots, R, \quad (24)$$

where  $R$  is the total number of the training samples, and  $G_u$  is the  $u$ -th decision tree. The XGBoost objective function is expressed as

$$Obj = \sum_{i=1}^R l(V_i, \hat{V}_i) + \sum_{u=1}^U \Omega(G_u). \quad (25)$$

In this expression, the first term  $l(V_i, \hat{V}_i)$  represents the conventional loss function, which quantifies the residual (error) between the measured speed  $V_i$  and the predicted speed  $\hat{V}_i$ . The second term  $\Omega(G_u)$

evaluates the complexity of each tree, which is influenced by the structure of the decision trees. XGBoost employs an additive training method, iteratively incorporating each new tree based on the results from the previous iteration. At the  $\delta$ -th iteration, the loss function is evaluated as  $l(V_i^s, \hat{V}_i^{\delta-1} + G_\delta(\bar{\mathbf{X}}_{V_i}))$ , where  $G_\delta$  is the newly added tree in the  $\delta$ -th iteration. Traditional machine learning objective functions are generally limited in their ability to measure both model accuracy and computational efficiency. By including a complexity term, XGBoost finds a balance between model performance and training efficiency. Prior to model training, data preprocessing is carried out to ensure high-quality input data. Additionally, hyperparameter tuning is performed to maintain generalizability. Further details about hyperparameters can be found in [Chen and Guestrin \(2016\)](#).

### 4.3. Model establishment and evaluation

This study used Bayesian optimization to determine the optimal combination of XGBoost hyperparameters. The considered hyperparameters and the corresponding tuning domains of the XGBoost modeling are listed in [Table 4](#). The processed data was divided into training and test sets, with five individual voyages reserved exclusively for testing. During model training, five-fold cross-validation was

Table 4

Hyperparameters used in XGBoost modeling and tuning ranges applied in this study.

Parameter	Tuning domain
Step size (learning rate)	[0.01, 1]
Maximum depth of a tree	[3, 12]
Number of trees	[500, 5000]
Minimum loss reduction required to make a split	[0, 3]
L1 regularization term	[0, 50]
L2 regularization term	[0, 50]
Minimum sum of instance weight required in a child	[0, 10]
Subsample ratio	[0.5, 1]

employed to identify the optimal hyperparameters through Bayesian optimization. The final hyperparameter configurations for both the speed prediction model and the fuel consumption rate prediction model are provided in [Appendix Table A3](#).

To evaluate model performance on the test set, root mean square error (RMSE) and mean absolute percentage error (MAPE) were used as evaluation metrics. The fuel consumption rate prediction model achieved an RMSE of 0.1877 and a MAPE of 0.87 %, while the speed prediction model yielded an RMSE of 0.5727 and a MAPE of 3.66 %. [Fig. 12](#) presents the prediction results of the two test voyages compared with the corresponding measured data. The left figures illustrate the results for a voyage exceeding 3000 km across the Baltic Sea and North Sea, while those on the right show the results for a voyage over 2000 km across the North Sea and English Channel.

As [Fig. 12](#) shows, the XGBoost models demonstrate a good ability to predict  $m_{fuel}$ , with predictions closely matching actual measurements across the example voyages, thereby validating the features used and hyperparameters tuned in the model. The predictive accuracy for  $m_{fuel}$  is expected, as the model is informed by key operational variables, such as propulsion power, which is highly correlated with fuel consumption. However, predicting ship speed  $V$  presents larger challenges. While the model successfully captures general trends, it struggles to match the peaks and valleys observed in actual measurements. This discrepancy may be attributed to the high variability of metocean conditions or the exclusion of other operational variables. Nevertheless, the established models accurately capture the overall trend without significant prediction errors, making it sufficient for use in subsequent power allocation optimization.

## 5. Results and discussions

In this section, the MS-PELT segmentation approach is first compared with the TICC algorithm for voyage segmentation to identify the advantages and limitations of each method, as well as to evaluate their performance. Then numerical experiments are conducted to evaluate the proposed voyage segmentation and power allocation optimization framework. The results are compared to measured data to assess the potential CO<sub>2</sub> emission reduction achieved through optimal power allocation. Since the case study chemical tanker mainly operates in short sea shipping routes within the Baltic Sea, North Sea, and English Channel, the emission factor  $r_{co_2}$  is set at 3.151 tons of CO<sub>2</sub> per ton of

fuel, based on light fuel oil (LFO) by [IMO \(2022\)](#) recommendations.

### 5.1. Comparison between TICC and proposed MS-PELT method for voyage segmentation

In this subsection, the TICC and proposed MS-PELT methods are applied for voyage segmentation comparison. The goal is to evaluate the strengths and weaknesses of each method and determine which approach is more suitable for generating legs in the power allocation optimization process. For comparison and analysis, both methods are applied to two example voyages, as shown in [Fig. 13](#). The sailing time for Voyage 1 ([Fig. 13 \(a\)](#)) is approximately 143 h, while that for Voyage 2 ([Fig. 13 \(b\)](#)) is 108 h.

The segmentation process incorporates metocean conditions encountered during Monte Carlo simulated voyages. The metocean variables for all simulated voyages are presented in [Fig. 14](#) for both example voyages. The orange dashed line represents the mean value of each metocean variable across all simulated voyages. As shown in the figure, although the speed profiles of each simulated voyage are randomly generated and vary, the general trend of the encountered metocean conditions is similar, with only variations in peak values and slight shifts in time at different waypoints. Finally, the metocean data from the simulated voyages is used to derive the ensemble metocean score, as defined in [Eq. \(3\)](#), for MS-PELT segmentation, while the mean value of the metocean data is used for TICC segmentation.

[Fig. 15](#) presents the segmentation results for Voyage 1, based on metocean conditions using MS-PELT ([Fig. 15 \(a\)](#)) and TICC ([Fig. 15 \(b\)](#)). Both methods successfully identify and isolate the peak variations of  $H_s$ ,  $V_{wind}$ , and  $V_{current}$ , along with their relative directions. These clusters represent areas where metocean conditions exhibit significant temporal and spatial variability, which is crucial for effective power allocation planning to ensure energy efficiency. For MS-PELT, the segmentation results tend to form relatively larger and more stable segments, providing a clear and straightforward division of the voyage into coherent legs. In contrast, the TICC method yields several smaller segments, particularly at the beginning of the voyage, resulting in more frequent power adjustments. [Fig. 16](#) illustrates the segmented trajectories produced by each method, providing a visual comparison of how the different clustering approaches translate into segmented routes. Additionally, the computational efficiency of each method varies significantly. The running time for MS-PELT is approximately 30 ms,

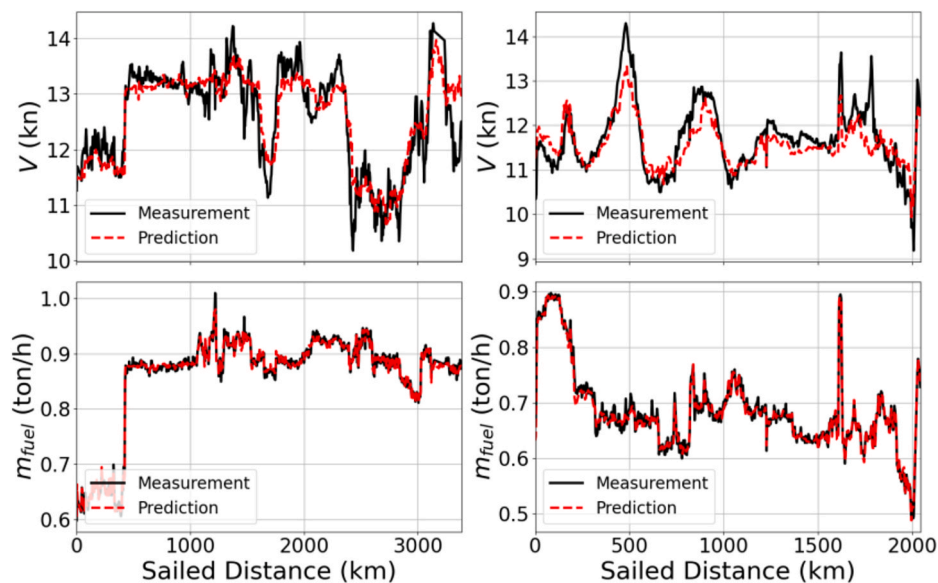


**Fig. 12.** Comparison of predicted and measured results for two validation voyages: one across the Baltic Sea and North Sea (left), and the other across the North Sea and English Channel (right).

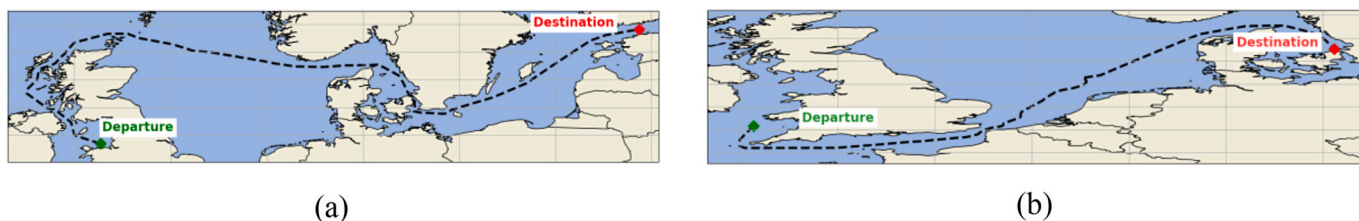


Fig. 13. Two example voyages for segmentation comparison: (a) Voyage 1, and (b) Voyage 2.

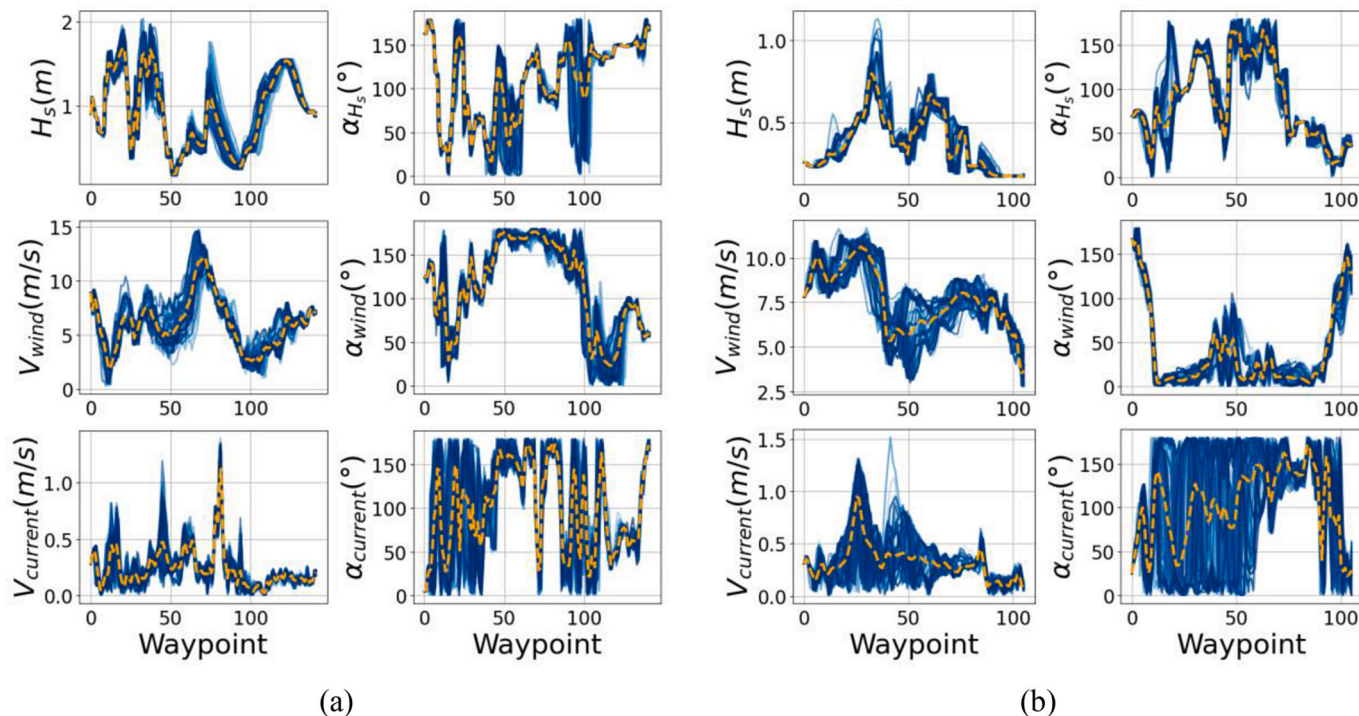


Fig. 14. Metocean conditions encountered during Monte Carlo simulated voyages for (a) Voyage 1 and (b) Voyage 2. The orange dashed line represents the mean value of each metocean variable across all simulated voyages along the route. (For interpretation of the references to colour in this figure legend, the reader is referred to the Web version of this article.)

whereas TICC takes around 50 s.

Similarly, the segmentation results for Voyage 2 are presented in Fig. 17, using MS-PELT (Fig. 17 (a)) and TICC (Fig. 17 (b)). The MS-PELT method produces relatively larger, more stable segments, providing a straightforward division of the voyage into coherent legs. However, TICC still generates more numerous and smaller segments, which require more frequent power adjustments, increasing operational complexity and burdening the crew. These frequent changes can also lead to increased CO<sub>2</sub> emissions due to more frequent shifting between different power levels. Fig. 18 visualizes the segmented trajectories derived from both methods. For computational efficiency, MS-PELT completes the segmentation in about 30 ms, while TICC requires approximately 50 s.

In practice, TICC requires specifying the number of clusters in the data. If this number is too large or too small, the method may fail to converge, resulting in no segmentation, posing a challenge in real-world applications where the number of clusters is not known. In contrast, MS-PELT does not require specifying the number of clusters, but instead uses a penalty factor  $\gamma$  to automatically detect change points. In this study, the factor is calculated as  $\gamma = (0.25a)^{(1-\text{Sensitivity})} \cdot 2 \log a$ , where  $a$  is the total number of waypoints of the voyage. A higher sensitivity (in the range of [0,1]) corresponds to a lower penalty, enhancing the algorithm's ability to detect change points. In this study, sensitivity is set to

1, resulting in a penalty of  $2 \log a$ , equivalent to using the Bayesian information criterion.

This formulation enhances the practicality of the MS-PELT algorithm by removing the need to predefine clustering parameters, making it more accessible in applications using real-time weather forecasts where such prior information is unavailable. In terms of efficiency, MS-PELT employs an effective pruning technique that eliminates unlikely change points early in the process, significantly reducing computational load. As a result, segmentation can be completed in approximately 30 ms, making the method highly suitable for real-time or near-real-time applications, especially in dynamic maritime environments. Therefore, the proposed MS-PELT method not only improves robustness in the presence of uncertainty but also provides segmented legs efficiently, which are then used in the subsequent power allocation optimization.

### 5.2. Propulsion power allocation optimization for voyages across the Baltic Sea and North Sea

For voyages across the Baltic Sea and the North Sea, four individual voyages, illustrated in Fig. 19, are selected as case studies to validate the proposed propulsion power allocation method. Detailed voyage information is provided in Table 5.

Since the case study vessel did not record emission information directly, we employed a consistent calculation approach to ensure a fair

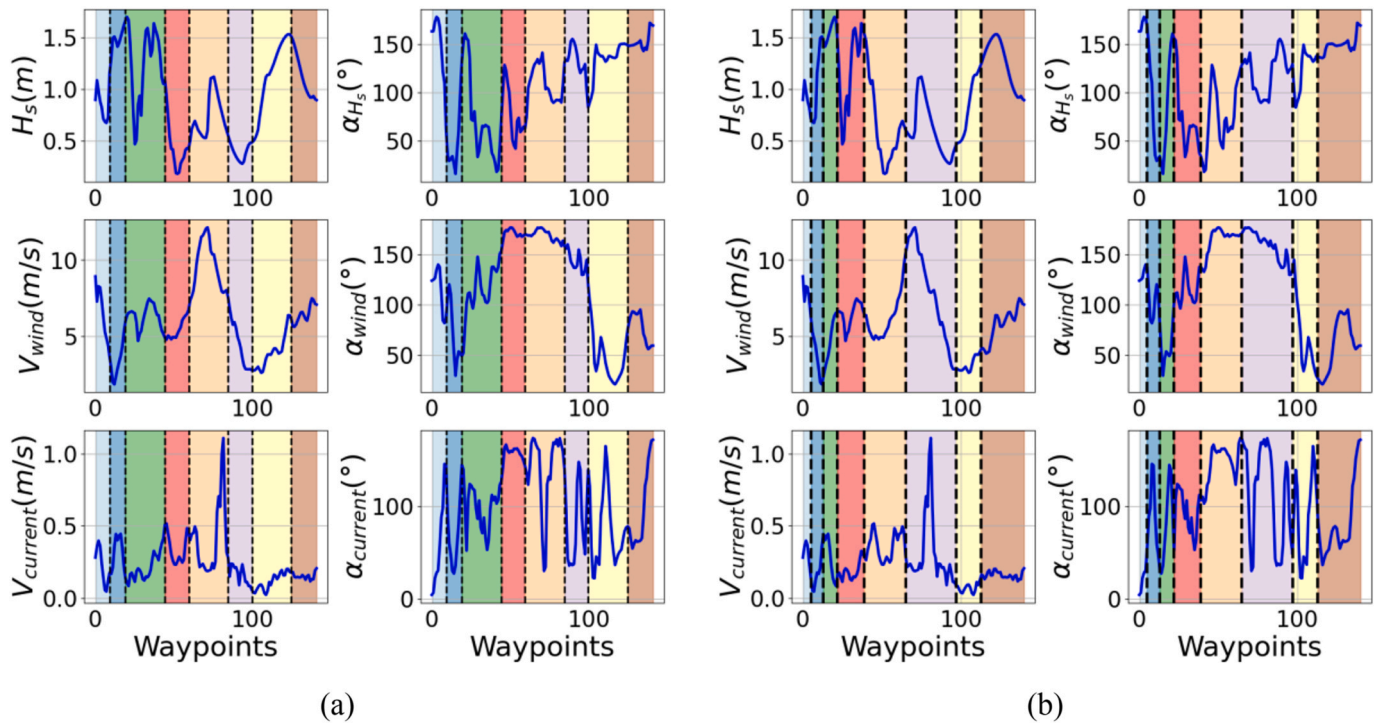


Fig. 15. Segmentation results for Voyage 1 based on metocean conditions using (a) MS-PELT and (b) TICC methods.

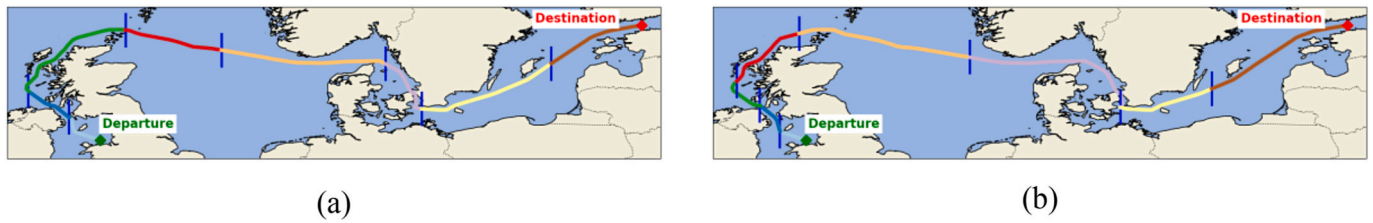


Fig. 16. Segmented trajectories for Voyage 1 using (a) MS-PELT and (b) TICC methods.

comparison between the optimized power allocation and the actual settings. Specifically, the emissions for the real voyage are calculated using the same method applied during optimization. This involves predicting fuel consumption using the machine learning model, and combining the predicted fuel consumption with the emission factor  $r_{CO_2}$  to obtain the  $CO_2$  emissions. Cases 1 and 2 feature relatively long routes, each spanning more than 3000 km and lasting over 140 h. By contrast, Cases 3 and 4, which take place solely within the Baltic Sea, cover shorter distances of around 1100 km and require approximately 60 and 55 h.

For Case 1 and Case 2, the voyage segmentation results are presented in Fig. 20. The power allocation optimization results are shown in Fig. 21 for Case 1 and Fig. 22 for Case 2, respectively. These figures illustrate the measured propulsion power and speed during the actual voyages, the optimized power settings for each leg, and the corresponding speeds. The metocean data encountered during the optimized voyage are also presented for a more comprehensive analysis.

As shown in Fig. 20 (a), the voyage in Case 1 is segmented into nine legs. The chemical tanker encountered relatively harsh weather conditions, with  $H_s$  reaching 3 m in legs 7 (purple) and 8 (yellow). Under this condition, the power allocation optimization achieved a potential  $CO_2$  emission reduction of 27.6 tons, which represents a reduction of 7.2 % compared to the actual voyage measurement. As seen in Fig. 21, the optimal power allocation strategy prioritizes increased power at the beginning of the voyage when the encountered wave conditions were

milder, followed by a significant reduction in power settings during leg 8 to conserve fuel. Although  $H_s$  was relatively high, the power setting was still increased in leg 7 due to favorable following wave conditions, which has a smaller wave resistance relative to bow sea and head sea. The actual voyage duration was around 145 h, while the optimized strategy introduced a minor delay of 17 min, well within the acceptable range of 1 %.

Similarly, for the voyage in Case 2, as shown in Fig. 20 (b) and 22, the voyage is segmented into eight legs. Among these segments, legs 2 (blue), 3 (green), 7 (yellow), and 8 (brown) experience peak  $H_s$  value exceeding 1.5 m. In leg 5 (orange), the chemical tanker encountered wind speed  $V_{wind}$  exceeding 10 m/s, and current speed  $V_{current}$  greater than 1 m/s. The optimal power allocation strategy involved reducing power during legs 3, 5, and 6 (purple), where conditions were least favorable (e.g., high waves and strong head wind). Conversely, power was increased during leg 2 with a following wave and leg 7, which had relatively mild wind conditions. Compared to the actual power settings, this optimized strategy resulted in a  $CO_2$  emission reduction of 12.3 tons, which is approximately a 4.5 % reduction, with a minor delay of only 5 min.

The detailed optimized  $CO_2$  emissions and time delays are presented in Table 6. For the shorter Baltic Sea voyages Case 3 and Case 4, the time delays after power allocation optimization also remain under 0.3 %, fulfilling the requirement that the total sailing time deviate by no more than 1 % from the ETA. Additionally, the emissions are reduced by 7.1 %

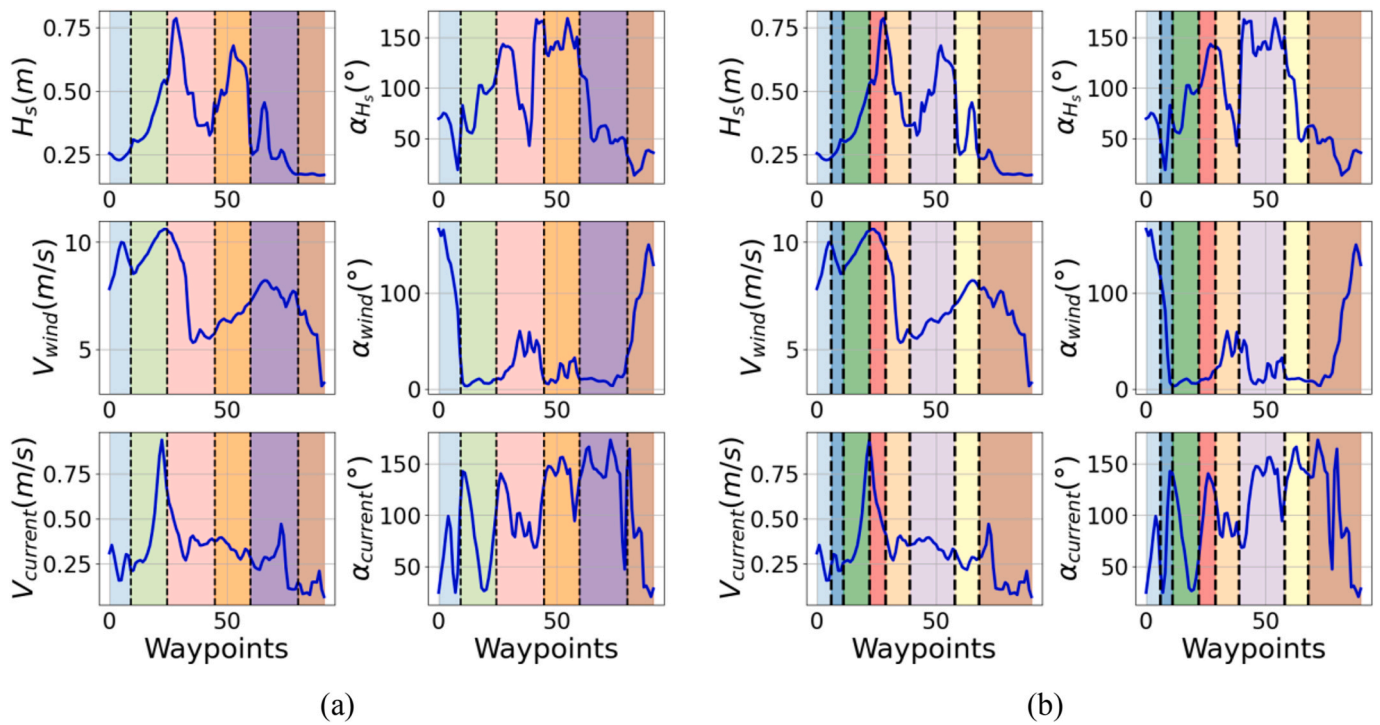


Fig. 17. Segmentation results for Voyage 2 based on metocean conditions using (a) MS-PELT and (b) TICC methods.

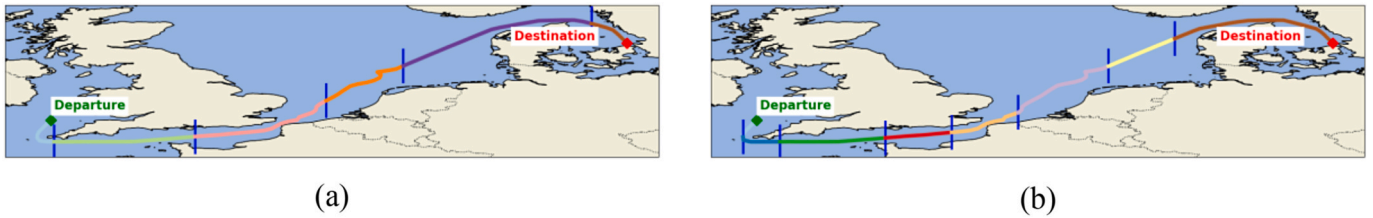


Fig. 18. Segmented trajectories for Voyage 2 using (a) MS-PELT and (b) TICC methods.

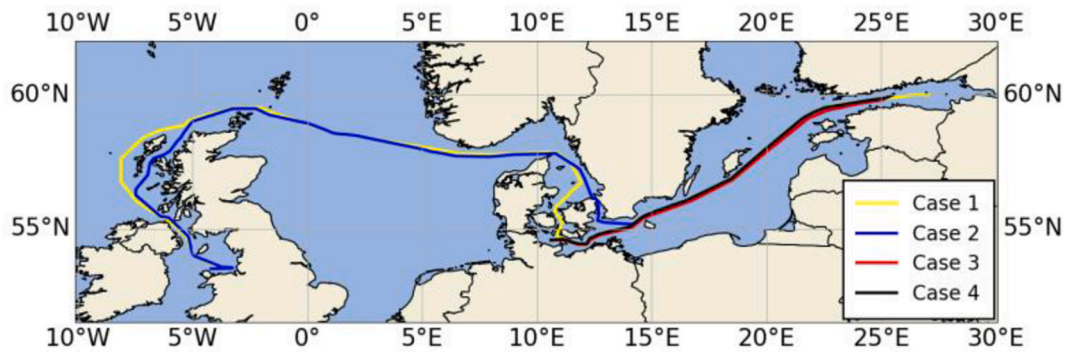


Fig. 19. The case study voyages across the Baltic Sea and North Sea applied for propulsion power allocation optimization.

and 7.3 %, respectively. The segmentation times for all case studies are approximately 30 ms. The optimization takes about 90 s for Cases 1 and 2, and around 35 s for Cases 3 and 4. Furthermore, an evaluation of the operative feasibility of the proposed propulsion power allocation was conducted. The sailing distances of each segment in Case 1 and Case 2 range from 191 km to 699 km, with corresponding sailing times between 9 and 30 h. These ranges confirm that the optimized power settings can be practically maintained throughout the voyages, ensuring that the proposed strategy is applicable under real operational conditions.

### 5.3. Propulsion power allocation optimization for voyages passing the English Channel

Similarly, four individual voyages passing through the English Channel are selected to verify the proposed method, as shown in Fig. 23. Detailed voyage information is presented in Table 7. Case 6 is relatively long, spanning over 2000 km and requiring more than 100 h to reach its ETA. In contrast, Case 8 is the shortest route, covering less than 1000 km and taking only about 47 h. Cases 5 and 7 share the same departure and

**Table 5**

The sailing information of the case study voyages across the Baltic Sea and North Sea.

Case ID	Sailing area	Distance [km]	ETA [hours]	Actual CO <sub>2</sub> emissions [tons]
1	Baltic and North Sea	3388	145.50	383.16
2	Baltic and North Sea	3089	143.83	271.68
3	Baltic	1118	60.50	83.06
4	Baltic	1153	55.33	90.24

destination, and their sailing trajectories largely overlap, the sailing time is around 80 h.

For voyages passing through English Channel such as Case 5 and Case 6, the ship typically encounters much calmer wave conditions. In this sailing condition, wind becomes an important factor affecting power allocation. The segmentation results for these two voyages are shown in Fig. 24. Fig. 25 presents the power allocation optimization results for Case 5, while Fig. 26 shows the results for Case 6.

As seen in Fig. 24 (a) and 25, the voyage in Case 5 is divided into six segments. During this voyage, the encountered wave conditions were relatively calm, with peak  $H_s$  value reaching approximately 0.7 m. In this context, wind conditions were the dominant factor affecting the ship's performance. During leg 1 (blue), which experienced wind speeds  $V_{wind}$  exceeding 10 m/s (mainly as bow wind or head wind), the power allocation optimization strategy reduced the power setting to lower emissions. As wind speeds gradually decreased in the subsequent legs, the optimized power settings increased accordingly. However, in leg 5 (purple), where wind speeds increased again, the power setting was adjusted downward to maintain energy efficiency. Compared to the

actual power settings, this optimized strategy saved 33.1 tons of emission, equivalent to a reduction of 14.5 %, while only incurring a delay of 11 min, corresponding to an increase of just 0.22 % in total sailing time.

For Case 6, the voyage has been segmented into six legs, as shown in Fig. 24 (b) and 26. The chemical tanker encountered a maximum  $H_s$  of less than 1 m, which still qualifies as very calm sea conditions. Similar to Case 5, wind speed  $V_{wind}$  and relative wind angle  $\alpha_{wind}$  primarily determined the power allocation optimization strategy. In leg 1 (blue), wind speeds exceeded 10 m/s and were near head wind, which led the optimization to choose a relatively lower power setting. In leg 2 (green), as the wind direction changed to following wind, and in leg 3 (red), as wind speed decreased, the power setting was gradually increased. However, in leg 4 (orange), the relative wave angle shifted to head sea, and in leg 5 (purple), wind speed increased again. The power allocation optimization opted to reduce power settings to improve energy efficiency. Compared to the actual power settings, this optimized strategy led to an emission reduction of 16.8 tons (approximately 9.5 %), with a minor delay of only 35 min.

The detailed optimized CO<sub>2</sub> emissions and time delays for the voyages passing through the English Channel are presented in Table 8. In both the extensively discussed Cases 5 and 6, as well as Cases 7 and 8, the time delay remains within 1 % of the ETA. Moreover, for Cases 7 and 8, the emissions are reduced by 4.9 % and 8.9 %, respectively, also confirming the effectiveness of the proposed framework. The segmentation times for all case studies are approximately 30 ms. The optimization process takes about 60 s for Case 6, around 40 s for Cases 5 and 7, and only about 30 s for Case 8. Similarly, for Case 5 and Case 6, which involve voyages across the English Channel, the sailing distances of each segment range from 196 km to 435 km, with sailing times between 8 and 19 h. These ranges also support the operational feasibility of the optimized propulsion power allocation.

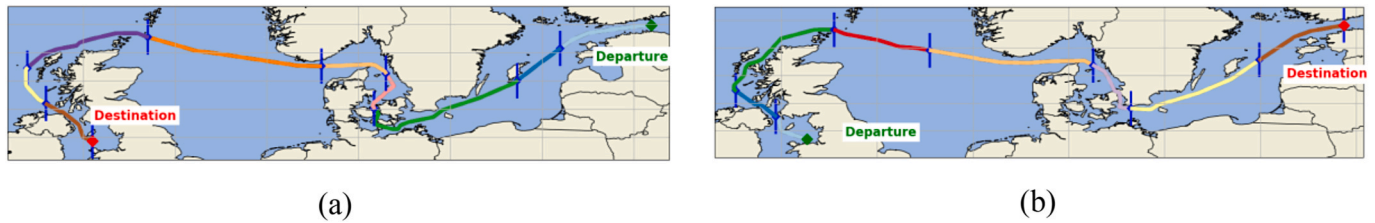


**Fig. 20.** Segmented trajectories for voyages across the Baltic Sea and North Sea, showing (a) Case 1 and (b) Case 2.

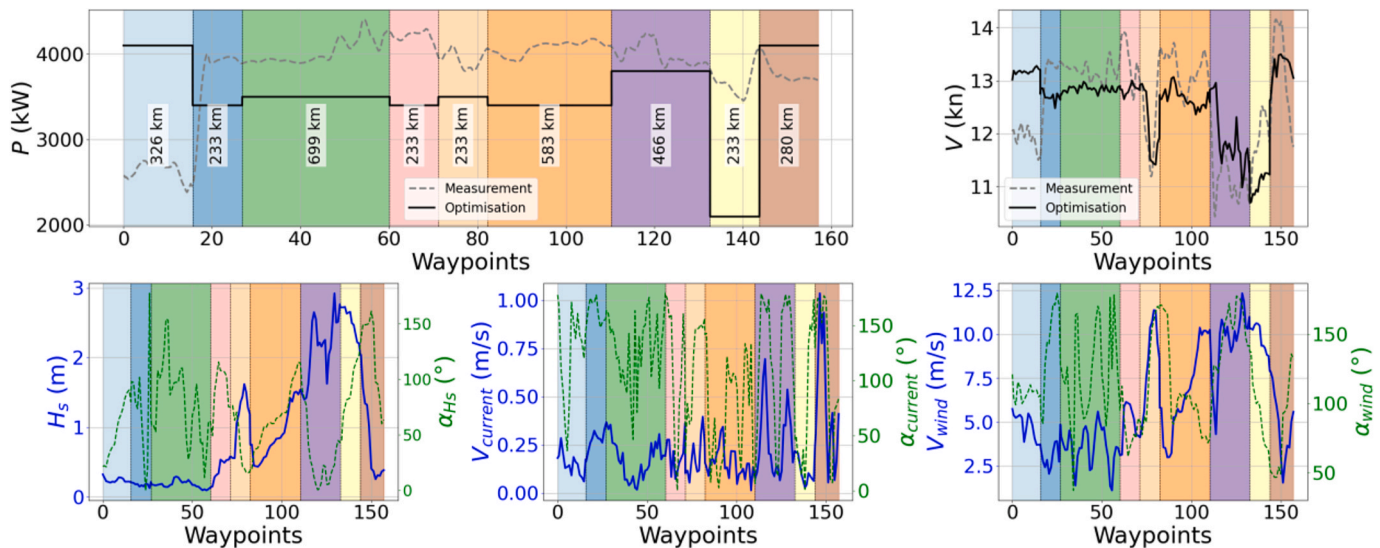


**Fig. 21.** Power allocation results for Case 1, including measured and optimized propulsion power, ship speed, and encountered meteocean conditions for each waypoint along the optimized voyage. The sailing distance of each segment is also indicated.

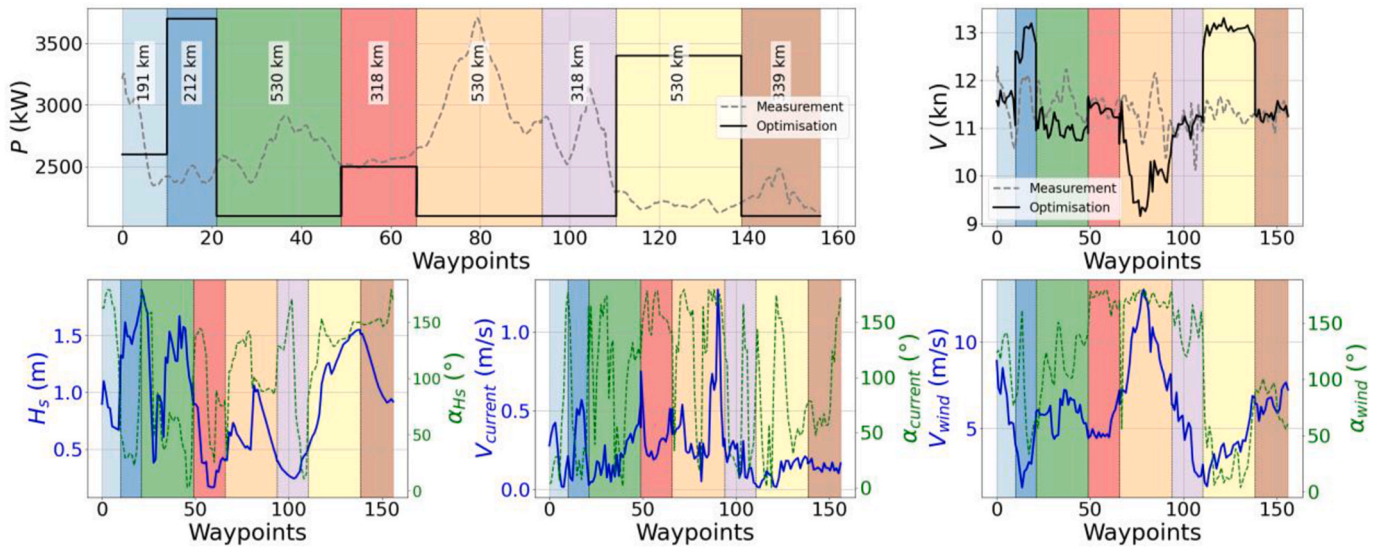


**Fig. 22.** Power allocation results for Case 2, including measured and optimized propulsion power, ship speed, and encountered meteocean conditions for each waypoint along the optimized voyage. The sailing distance of each segment is also indicated.

**Table 6**

The optimized CO<sub>2</sub> emissions and time delay of the case study voyages across the Baltic Sea and North Sea.

Case ID	Time delay [%]	Optimized CO <sub>2</sub> emissions [tons]	Emissions reduction [%]
1	0.19 %	355.56	7.2 %
2	0.06 %	259.42	4.5 %
3	0.28 %	77.14	7.1 %
4	0.10 %	83.63	7.3 %

**5.4. Discussion of SSS emission reduction by this method and other measures**

From the global shipping perspectives, the 2023 IMO GHG strategy (IMO, 2023) envisages technical, operational and economic measures to reduce shipping emissions. According to the fourth IMO GHG Study (IMO, 2020), about 64 % CO<sub>2</sub> reduction from shipping in 2050 will be achieved by alternative fuels, while the third IMO GHG study (IMO, 2014) presented an average daily CO<sub>2</sub> emission reduction of 27 % for a 12 % speed decrease. For short sea shipping, Degiuli et al. (2021) reported that a 13.6 % speed reduction resulted in approximately 31 % CO<sub>2</sub> emission reduction in the Mediterranean Sea. Degiuli et al. (2024) investigated the impact of slow steaming on a Panamax container ship and found that a 10 % speed reduction can lead to an annual CO<sub>2</sub> emission decrease of approximately 16.9 %. Dantas and Theotokatos (2023) estimated that CO<sub>2</sub> emissions can be reduced by approximately 4

% for transition autonomous short-sea sailing ships equipped with more advanced autonomous control, and by 8–11 % for Next Generation Autonomous Ships that operate without a crew accommodation compartment. For other ship operation related measures, a systematic review by Bouman et al. (2017) reported on average from 5 to 20 % CO<sub>2</sub> emission reduction from e.g., wind propulsion, speed and voyage optimization, etc. In comparison with our proposed method for optimal power allocation along individual voyages, the case studies show from 4.5 % to 14.5 % CO<sub>2</sub> emission reduction, while maintaining the original ETA and without compromising transport efficiency. It may not be as efficient as the alternative fuel and slow steaming measures, but our proposed method can be easily combined with those two measures to further reduce fuel consumption/emissions. For example, if shipowners

**Table 7**

The sailing information of the case study voyages passing through the English Channel.

Case ID	Sailing area	Distance [km]	ETA [hours]	Actual CO <sub>2</sub> emissions [tons]
5	English Channel	1718	80.33	176.90
6	English Channel	2043	108.50	223.41
7	English Channel	1712	78.00	147.47
8	English Channel	980	47.00	67.10

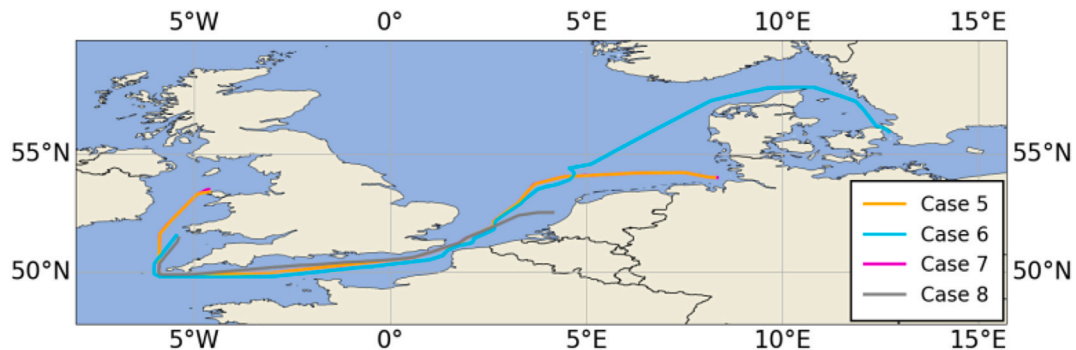


**Fig. 23.** The case study voyages passing through the English Channel applied for power allocation optimization.

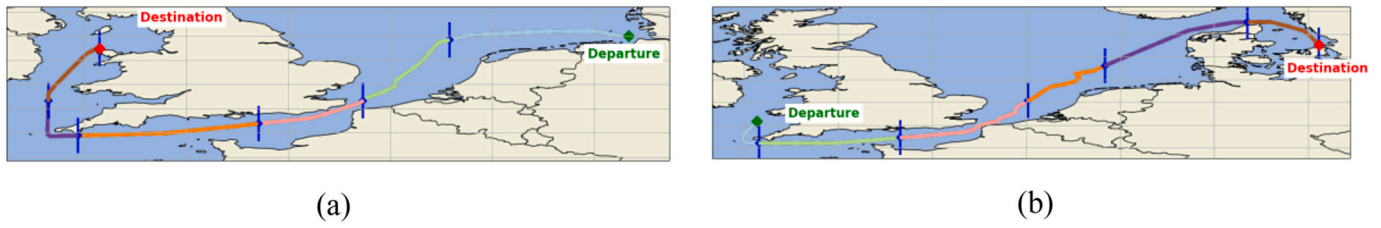


Fig. 24. Segmented trajectories for voyages passing through the English Channel, showing (a) Case 5 and (b) Case 6.

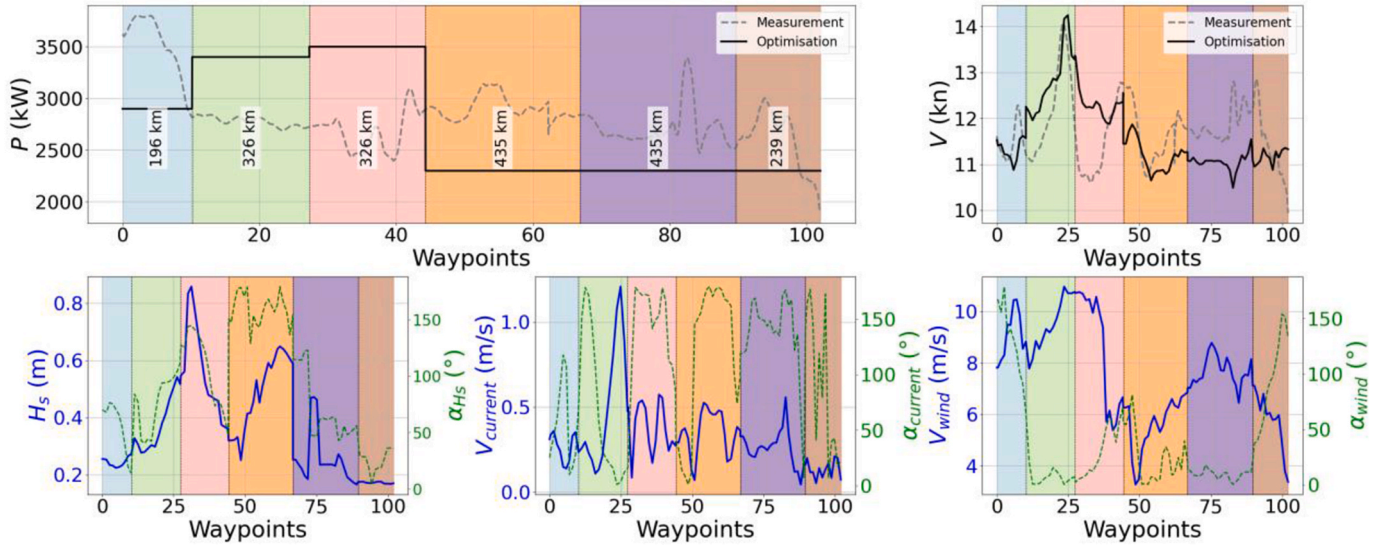


Fig. 25. Power allocation results for Case 5, including measured and optimized propulsion power, ship speed, and encountered metocean conditions for each waypoint along the optimized voyage. The sailing distance of each segment is also indicated.

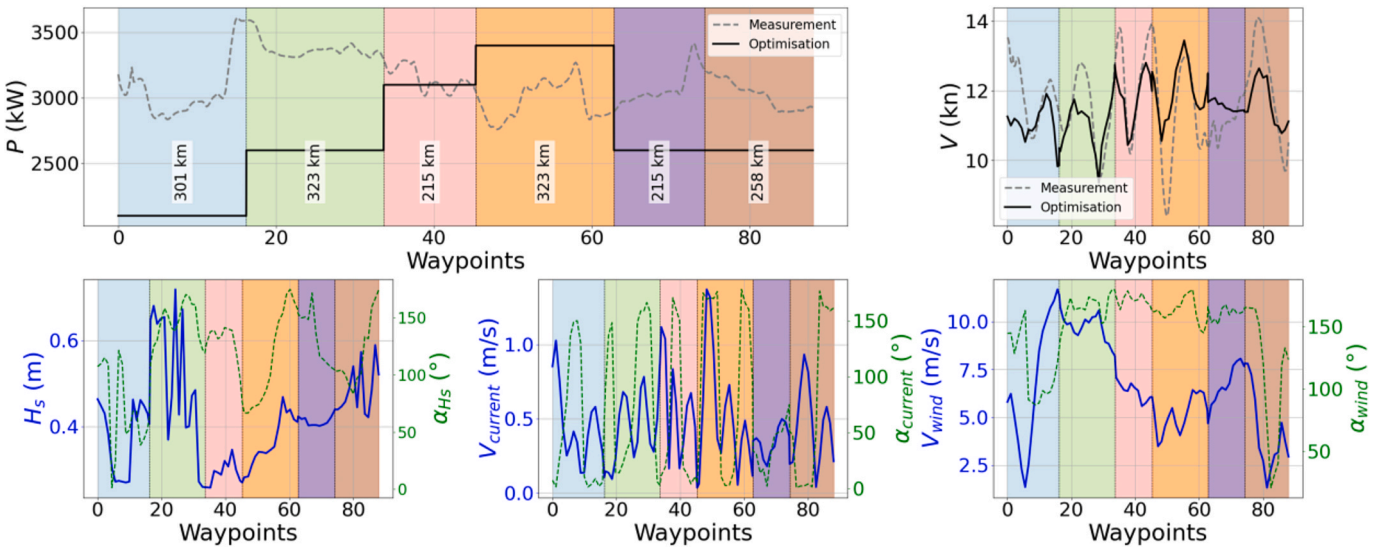


Fig. 26. Power allocation results for Case 6, including measured and optimized propulsion power, ship speed, and encountered metocean conditions for each waypoint along the optimized voyage. The sailing distance of each segment is also indicated.

choose to apply slow steaming, the proposed methods of segmentation and propulsion power allocation framework can be readily adapted to accommodate longer sailing times and lower average speeds. In this way, it can also serve as a supporting tool to enhance the environmental benefits of slow steaming, potentially enabling even greater CO<sub>2</sub> reductions.

## 6. Conclusion

This study proposes a two-stage optimization framework for ship power allocation in short sea shipping. In the first stage, voyage segmentation is performed using a metocean score-based PELT algorithm. This approach divides the voyage into several legs based on metocean conditions, minimizing frequent power adjustments and simplifying

**Table 8**

The optimized CO<sub>2</sub> emissions and time delay of the case study voyages passing through the English Channel.

Case ID	Time delay [%]	Optimized CO <sub>2</sub> emissions [tons]	Emissions reduction [%]
5	0.73 %	160.07	9.5 %
6	0.17 %	190.32	14.5 %
7	-0.19 %	140.22	4.9 %
8	0.27 %	62.93	8.9 %

both the allocation process and computational complexity. In the second stage, a parallel coupling DP method is employed to optimize the power allocation of each leg efficiently across the entire voyage, using the segmented output from the first stage and machine learning-based ship performance models. Using three years of full-scale measurements of a case study chemical tanker operating in short sea shipping, the key findings of this study are summarized as follows:

- Compared to the state-of-the-art multivariate clustering algorithm TICC, the proposed MS-PELT method is more practical and efficient, avoiding the creation of numerous small legs that would otherwise increase the frequency of power setting changes.
- The proposed power allocation optimization by a novel parallel coupling DP approach has demonstrated promising CO<sub>2</sub> emission reduction, with an average environmental impact reduction of around 8 % and the largest arrival delay of only 0.73 %.
- The proposed framework demonstrates high computational efficiency, with voyage segmentation typically requiring only 30 ms and power allocation optimization just around 1 min, making it a suitable choice for real-time or near-real-time applications.

In real-world operations of the case study vessel, propulsion power varies frequently along a voyage due to changes in speed and encountered metocean conditions. Such frequent adjustments can significantly increase engine wear and reduce thermal efficiency. While some ocean-crossing shipping companies have already adopted constant-power strategies to mitigate these issues, applying a fully constant power setting is often not feasible in short sea shipping, where ETA constraints are stricter and weather forecasts more uncertain. To address this, the proposed method maintains constant propulsion power within each voyage segment rather than over the entire route. This segmented constant-power strategy provides a practical compromise: it reduces the frequency of power adjustments, helps extend engine life, improves operational efficiency, and still satisfies strict schedule requirements, making it well-suited for short sea shipping applications. The operative feasibility analysis demonstrated that the optimized propulsion power is technically practical for short sea shipping voyages, further validating the applicability of the proposed method. This work contributes to the advancement of integrating data-driven segmentation and dynamic

## Appendix A

**Table A1**

The proposed MS-PELT algorithm.

MS-PELT algorithm: voyage segmentation using ensemble metocean score based PELT algorithm
<b>Input:</b> The number of simulated referenced voyages $Q$ , minimum time length for a leg $\epsilon$ , predefined route longitudes and latitudes $(x, y)$ , voyage starting time $t_1$ , estimated time of arrival ETA
<b>Output:</b> Number of legs $n$ , route breakpoints $\tau = (\tau_1, \tau_2, \dots, \tau_b)$
1: Calculate the total distance $D$ of the predefined route, and the average speed $V_{\text{average}}$ to match the ETA
2: Initialize waypoints $[(x_1, y_1), (x_2, y_2) \dots (x_a, y_a)]$ with 1 h sailing distance interval at $V_{\text{average}}$ , extract metocean data $MO_{q,1}$ at location $(x_1, y_1)$ and time $t_1$ , calculate metocean score $MS_{q,1}$ as Eq. (2)
3: for $q = 1$ to $Q$ do

(continued on next page)

programming to enhance the energy efficiency of short sea shipping. It provides the maritime transportation industry with innovative tools and methodologies to optimize ship power settings during short sea voyages, reducing CO<sub>2</sub> emissions and environmental impact. Regarding the limitations of this study, the proposed method relies on a power-to-speed performance model, which may encounter challenges when segments experience unseen or rare metocean conditions in the training data, such as large waves. Under such conditions, the model's predictive accuracy may be compromised, affecting the reliability of sailing time estimation. This limitation is common to most existing ship operation optimization studies that utilize data-driven performance models. Furthermore, unlike the use of hindcast metocean data for voyage segmentation in this study, the proposed method's application in real-world navigation relies on weather forecasts. Forecasted data inherently carries uncertainties, which may increase over extended prediction periods. In practical applications, this may require segmentation and optimization to be recalibrated or updated every 1–2 days to maintain accuracy. The proposed framework's computational efficiency enables rapid re-optimization when substantial changes in weather forecasts occur. In addition, when defining the sailing time constraint, a large constraint margin was avoided, which would have changed the problem to a slow steaming scenario.

## CRedit authorship contribution statement

**Daniel Vergara:** Writing – original draft, Visualization, Validation, Software, Methodology, Investigation, Formal analysis, Conceptualization. **Xiao Lang:** Writing – review & editing, Writing – original draft, Supervision, Methodology, Investigation, Formal analysis. **Mingyang Zhang:** Writing – review & editing, Supervision, Investigation, Formal analysis. **Martin Alexandersson:** Writing – review & editing, Investigation, Formal analysis, Conceptualization. **Wengang Mao:** Writing – review & editing, Supervision, Project administration, Methodology, Funding acquisition, Conceptualization.

## Declaration of competing interest

The authors declare that they have no known competing financial interests or personal relationships that could have appeared to influence the work reported in this paper.

## Acknowledgments

This work was supported by the Trafikverket (Swedish Transport Administration) [grant No. TRV2023/98101]; the Vinnova (Swedish Governmental Agency for Innovation Systems) [grant No. 2021-02768]; and the Trafikverket/Lighthouse [grant No. FP4 2020]. The authors also grateful to the ship owners for providing the full-scale measurement data.

**Table A1** (continued)

---

MS-PELT algorithm: voyage segmentation using ensemble metocean score based PELT algorithm

---

4: Monte Carlo simulation generates speed profile  $\mathbf{V}_q = [V_{q,1}, V_{q,2}, \dots, V_{q,a-1}]$

5: **for**  $k = 2$  to  $a$  **do**

6: Compute arrival time on  $k$ -th waypoint  $t_k = \frac{d_{k-1-k}}{V_{q,k-1}} + t_{k-1}$ , extract metocean data  $\mathbf{MO}_{q,k}$  at location  $(x_k, y_k)$  and time  $t_k$ , calculate metocean score  $MS_{q,k}$  as Eq. (2)

7: **end for**

8: **end for**

9: **for**  $k = 1$  to  $a$  **do**

10: Calculate ensemble metocean score  $\overline{MS}_k$  as Eq. (3)

11: **end for**

12: Perform PELT segmentation with  $\varepsilon$  on  $\overline{MS}_{1,a}$

13: **Return**  $n$  and  $\tau$

---

**Table A2**

The proposed parallel coupled DP algorithm.

---

PCDP algorithm: propulsion power allocation optimization using parallel coupling DP algorithm

---

**Input:** Discrete set of propulsion power  $[\Gamma_1, \Gamma_2, \dots, \Gamma_e]$ , number of legs  $n$ , number of parallel scenarios  $H$ , minimum and maximum allowable speed  $V_{\min}, V_{\max}$

**Output:** Optimal power allocation setting  $\mathbf{P}_{\text{opt}}$  for each leg, minimum total emission

1: Initialize DP table DP to infinity, traceback table traceback to None, arrival.times to infinity

2: **for**  $j = 1$  to  $n$  **do**

3: **if**  $j = 1$  **do**

4: **for** each power setting  $\Gamma_i$  in  $[\Gamma_1, \Gamma_2, \dots, \Gamma_e]$  **do**

5: Extract metocean condition  $\mathbf{W}_{1,1}$  at location  $(x_{1,1}, y_{1,1})$  and time  $t_{1,1}$ , evaluate  $V_{1,1}, m_{\text{fuel}}$  based on power setting  $\Gamma_i$  and  $\mathbf{W}_{1,1}$

6: **for**  $k = 2$  to  $m_1 - 1$  **do**

7: Compute arrival time on  $k$ -th waypoint  $t_{1,k} = \frac{d_{k-1-k}}{V_{1,k-1}} + t_{j,k-1}$ , extract metocean condition  $\mathbf{W}_{1,k}$  at location  $(x_{1,k}, y_{1,k})$  and time  $t_{1,k}$ , evaluate  $V_{1,k}, m_{\text{fuel}}$  and based on power setting  $\Gamma_i$  and  $\mathbf{W}_{1,k}$

8: **end for**

9: **if**  $V_{\min} \leq V_{1,k} \leq V_{\max}$  **continue**

10: **for**  $k = 1$  to  $m_1 - 1$  **do**

11: Compute  $f_1$  based on Eq. (14)

12: **end for**

13: Update  $\text{DP}[1][0][\Gamma_i] = f_1$ ,  $\text{traceback}[1][0][\Gamma_i] = (0, \Gamma_i)$ , and store  $\text{arrival.times}[1][0][\Gamma_i] = t_{1,m_1}$

14: **end for**

15: **else** Compute the nominal departure time  $t_{j,1}^{(0)}$  as Eq. (17), max deviation time  $\Delta T_j$  as Eq. (20), parallel scenarios time interval  $\Delta t_j = \frac{\Delta T_j}{H-1}$

16: **for** each candidate  $h_i$  in  $\left[0, \pm 1, \pm 2, \dots, \pm \left\lfloor \frac{H}{2} \right\rfloor\right]$  **do**

17: Compute starting time  $t_{j,1} = t_{j,1}^{(h_i)}$  as Eq. (19)

18: **for** each power setting  $\Gamma_i$  in  $[\Gamma_1, \Gamma_2, \dots, \Gamma_e]$  **do**

19: **for**  $k = 2$  to  $m_j - 1$  **do**

20: Compute arrival time on  $k$ -th waypoint  $t_{j,k} = \frac{d_{k-1-k}}{V_{j,k-1}} + t_{j,k-1}$ , extract metocean condition  $\mathbf{W}_{j,k}$  at location  $(x_{j,k}, y_{j,k})$  and time  $t_{j,k}$ , evaluate  $V_{j,k}, m_{\text{fuel}}$  and based on power setting  $\Gamma_i$  and  $\mathbf{W}_{j,k}$

21: **end for**

22: **if**  $V_{\min} \leq V_{j,k} \leq V_{\max}$  **continue**

23: **for**  $k = 1$  to  $m_j - 1$  **do**

24: compute  $f_j$  based on Eq. (14)

25: **end for**

26: Update  $\text{DP}[j][h_i][\Gamma_i] = f_j$ ,  $\text{traceback}[j][h_i][\Gamma_i] = (h_i, \Gamma_i)$ , and store  $\text{arrival.times}[j][h_i][\Gamma_i] = t_{j,m_j}$

27: **end for**

28: **end for**

29: **end for**

30: **for**  $j = 1$  to  $n - 1$  **do**

31: **for** each scenario in  $\text{arrival.times}[j]$  **do**

32: Connect to one of the scenarios of the next leg with starting times  $t_{j+1,1}^{(h_i)}$ ,  $h_i \in \left[0, \pm 1, \pm 2, \dots, \pm \left\lfloor \frac{H}{2} \right\rfloor\right]$  based on closest time, store linked connections for later optimization.

33: **end for**

34: Apply DP to minimize emissions across all scenarios, and extract the optimal power allocation  $\mathbf{P}_{\text{opt}}$

35: Simulate the voyage using  $\mathbf{P}_{\text{opt}}$ , if  $0.99 \leq (t_{n,m_n}/\text{ETA}) \leq 1.01$  **break**

36: **else if** use the next best power combination and re-simulate, until ETA constraint is satisfied.

37: **Return**  $\mathbf{P}_{\text{opt}}$ , minimum total emission

---

**Table A3**  
Hyperparameters of the speed and fuel consumption rate prediction model.

Parameter	Speed model	Fuel model
Step size (learning rate)	0.1396	0.1643
Maximum depth of a tree	5	9
Number of trees	3343	4489
Minimum loss reduction required to make a split (gamma)	2.8806	0.1916
L1 regularization term (alpha)	0.3588	0.2529
L2 regularization term (lambda)	4.088	2.2814
Minimum sum of instance weight required in a child	1.4623	1.1818
Subsample ratio	0.9827	0.9882
Column subsample ratio	0.9632	0.9986

## Data availability

The authors do not have permission to share data.

## References

- Bellman, R., 1952. On the theory of dynamic programming. *Proc. Natl. Acad. Sci.* 38 (8), 716–719. <https://doi.org/10.1073/pnas.38.8.716>.
- Bouman, E.A., Lindstad, E., Rialland, A.I., Strømman, A.H., 2017. State-of-the-art technologies, measures, and potential for reducing GHG emissions from shipping – a review. *Transport. Res. Transport Environ.* 52, 408–421. <https://doi.org/10.1016/j.trd.2017.03.022>.
- Calvert, S., Deakins, E., Motte, R., 1991. A dynamic system for fuel optimization trans-ocean. *J. Navig.* 44, 233–265.
- Chen, T.Q., Guestrin, C., 2016. XGBoost: a scalable tree boosting system. *KDD'16: Proceedings of the 22nd ACM SIGKDD International Conference on Knowledge Discovery and Data Mining*, pp. 785–794. <https://doi.org/10.1145/2939672.2939785>.
- Copernicus, 2020. Copernicus Marine Environment Monitoring Service (CMEMS). European Commission. Retrieved from <https://marine.copernicus.eu>.
- CMEMS, 2023. Copernicus Marine Environment Monitoring Service: State of the Ocean Report 2023. Copernicus Marine Service. Retrieved from <https://marine.copernicus.eu>.
- Dantas, J.L.D., Theotokatos, G., 2023. A framework for the economic–environmental feasibility assessment of short-sea shipping autonomous vessels. *Ocean Eng.* 279, 114420. <https://doi.org/10.1016/j.oceaneng.2023.114420>.
- Degiuli, N., Martić, I., Farkas, A., Gospić, I., 2021. The impact of slow steaming on reducing CO<sub>2</sub> emissions in the Mediterranean Sea. *Energy Rep.* 7, 8131–8141. <https://doi.org/10.1016/j.egyr.2021.02.046>.
- Degiuli, N., Martić, I., Grlj, C.G., 2024. Slow steaming as a sustainable measure for low-carbon maritime transport. *Sustainability* 16, 11169. <https://doi.org/10.3390/su16211169>.
- Du, W., Li, Y., Zhang, G., Wang, C., Zhu, B., Qiao, J., 2022. Energy saving method for ship weather routing optimization. *Ocean Eng.* 258, 111771. <https://doi.org/10.1016/j.oceaneng.2022.111771>.
- Fagerholt, K., Gausel, N.T., Rakke, J.G., Psaraftis, H.N., 2015. Maritime routing and speed optimization with emission control areas. *Transport. Res. C Emerg. Technol.* 52, 57–73. <https://doi.org/10.1016/j.trc.2014.12.010>.
- Fan, A., Yang, J., Yang, L., Liu, W., Vladimir, N., 2022. Joint optimization for improving ship energy efficiency considering speed and trim control. *Transport. Res. Transport Environ.* 113, 103527. <https://doi.org/10.1016/j.trd.2022.103527>.
- Fan, A.L., Fan, X.L., Zhang, M.Y., Yang, L., Xiong, Y.Q., Lang, X., Sheng, C.X., He, Y.P., 2024. Data-driven ship typical operational conditions: a benchmark tool for assessing ship emissions. *J. Clean. Prod.* 483, 144252. <https://doi.org/10.1016/j.jclepro.2024.144252>.
- Fossen, T.I., 2002. *Marine Control Systems: Guidance, Navigation and Control of Ships, Rigs and Underwater Vehicles*, 8.4. Marine Cybernetics, Trondheim, Norway, pp. 340–365.
- Guericke, S., Tierney, K., 2015. Liner shipping cargo allocation with service levels and speed optimization. *Transport. Res. E Logist. Transport. Rev.* 84, 40–60. <https://doi.org/10.1016/j.trre.2015.10.002>.
- Han, Y.Y., Ma, W.H., Ma, D.F., 2023. Green maritime: an improved quantum genetic algorithm-based ship speed optimization method considering various emission reduction regulations and strategies. *J. Clean. Prod.* 385, 135414. <https://doi.org/10.1016/j.jclepro.2022.135814>.
- Hallac, D., Vare, S., Boyd, S., Leskovec, J., 2017. Toeplitz inverse covariance-based clustering of multivariate time series data. *Proceedings of the 23rd ACM SIGKDD International Conference on Knowledge Discovery and Data Mining (KDD '17)*. ACM, New York, NY, USA, pp. 215–223. <https://doi.org/10.1145/3097983.3098060>.
- International Maritime Organization, 2020. Fourth IMO Greenhouse Gas Study 2020. International Maritime Organization. Retrieved from <https://www.imo.org/en/ourwork/Environment/Pages/Fourth-IMO-Greenhouse-Gas-Study-2020.aspx>.
- International Maritime Organization, 2014. Third IMO Greenhouse Gas Study 2014. International Maritime Organization. Retrieved from <https://www.imo.org/en/ourwork/environment/pages/greenhouse-gas-studies-2014.aspx>.
- International Maritime Organization, 2022. Resolution MEPC.364(79), 2022 guidelines on the method of calculation of the attained energy efficiency design index (EEDI) for new ships. Retrieved from <https://www.wcdn.imo.org/localresources/en/KnowledgeCentre/IndexofIMOResolutions/MEPCDocuments/MEPC.364%2879%29.pdf>.
- International Maritime Organization, 2023. Revised IMO strategy on reduction of greenhouse gas emissions from ships. Retrieved from <https://www.imo.org/en/MediaCentre/PressBriefings/pages/Revised-GHG-reduction-strategy-for-global-shipping-adopted.aspx>.
- Jeong, S., Kim, T., 2023. Generating a path-search graph based on ship-trajectory data: route search via dynamic programming for autonomous ships. *Ocean Eng.* 283, 114503. <https://doi.org/10.1016/j.oceaneng.2023.114503>.
- Jimenez, V.J., Kim, H., Munim, Z.H., 2022. A review of ship energy efficiency research and directions towards emission reduction in the maritime industry. *J. Clean. Prod.* 366, 132888. <https://doi.org/10.1016/j.jclepro.2022.132888>.
- Killick, R., Fearnhead, P., Eckley, I., 2012. Optimal detection of changepoints with a linear computational cost. *J. Am. Stat. Assoc.* 107 (500), 1590–1598. <https://doi.org/10.1080/01621459.2012.737745>.
- Kim, K.-I., Lee, K.-M., 2018. Dynamic programming-based vessel speed adjustment for energy saving and emission reduction. *Energies* 11 (5), 1273. <https://doi.org/10.3390/en11051273>.
- Kim, H.-J., Son, D.-H., Yang, W., Kim, J.-G., 2019. Liner ship routing with speed and fleet size optimization. *KSCIE J. Civ. Eng.* 23 (3), 1341–1350. <https://doi.org/10.1007/s12205-019-0564-6>.
- Lang, X., Wu, D., Mao, W., 2022. Comparison of supervised machine learning methods to predict ship propulsion power at sea. *Ocean Eng.* 245, 110387. <https://doi.org/10.1016/j.oceaneng.2021.110387>.
- Lang, X., Wu, D., Mao, W., 2024. Physics-informed machine learning models for ship speed prediction. *Expert Syst. Appl.* 238, 121877. <https://doi.org/10.1016/j.eswa.2023.121877>.
- Laurie, A., Anderlini, E., Dietz, J., Thomas, G., 2021. Machine learning for shaft power prediction and analysis of fouling related performance deterioration. *Ocean Eng.* 234, 108886. <https://doi.org/10.1016/j.oceaneng.2021.108886>.
- Lee, S.-J., Sun, Q., Meng, Q., 2023. Vessel weather routing subject to sulfur emission regulation. *Transport. Res. E Logist. Transport. Rev.* 177, 103235. <https://doi.org/10.1016/j.trre.2023.103235>.
- Li, X., Sun, B., Guo, C., Du, W., Li, Y., 2020. Speed optimization of a container ship on a given route considering voluntary speed loss and emissions. *Appl. Ocean Res.* 94, 101995. <https://doi.org/10.1016/j.apor.2019.101995>.
- Li, X., Sun, B., Jin, J., Ding, J., 2022. Speed optimization of container ship considering route segmentation and weather data loading: turning point-time segmentation method. *J. Mar. Sci. Eng.* 10 (12), 1835. <https://doi.org/10.3390/jmse10121835>.
- Li, X., Sun, B., Jin, J., Ding, J., 2023. Ship speed optimization method combining fisher optimal segmentation principle. *Appl. Ocean Res.* 140, 103743. <https://doi.org/10.1016/j.apor.2023.103743>.
- Luo, X., Yan, R., Wang, S.N., 2023. Comparison of deterministic and ensemble weather forecasts on ship sailing speed optimization. *Transport. Res. Transport Environ.* 121, 103801. <https://doi.org/10.1016/j.trd.2023.103801>.
- Ma, W.H., Ma, D.F., Ma, Y.J., Zhang, J.F., Wang, D.H., 2021. Green maritime: a routing and speed multi-objective optimization strategy. *J. Clean. Prod.* 305, 127179. <https://doi.org/10.1016/j.jclepro.2021.127179>.
- Papadimitriou, S., Lyridis, D.V., Kolioussis, I.G., Tsioumas, V., Sdoukopoulos, E., Stavroulakis, P.J., 2019. *The Dynamics of Short Sea Shipping: New Practices and Trends*. Palgrave Macmillan.
- Psaraftis, H.N., Kontovas, C.A., 2014. Ship speed optimization: concepts, models and combined speed-routing scenarios. *Transport. Res. C Emerg. Technol.* 44, 52–69. <https://doi.org/10.1016/j.trc.2014.03.001>.
- Qi, X., Song, D.-P., 2012. Minimizing fuel emissions by optimizing vessel schedules in liner shipping with uncertain port times. *Transport. Res. E Logist. Transport. Rev.* 48 (4), 863–880. <https://doi.org/10.1016/j.trre.2012.02.001>.
- Shang, C., Fu, L., Bao, X., Xiao, H., Xu, X., Hu, Q., 2024. Dynamic joint optimization of power generation and voyage scheduling in ship power system based on deep reinforcement learning. *Elec. Power Syst. Res.* 229, 110165. <https://doi.org/10.1016/j.epr.2024.110165>.

- Shao, W., Zhou, P., Thong, S.K., 2012. Development of a novel forward dynamic programming method for weather routing. *J. Mar. Sci. Technol.* 17, 239–251. <https://doi.org/10.1007/s00773-011-0152-z>.
- Shu, Y.Q., Han, B.Y., Song, L., Yan, T., Gan, L.X., Zhu, Y.X., Zheng, C.M., 2024. Analyzing the spatio-temporal correlation between tide and shipping behavior at estuarine port for energy-saving purposes. *Appl. Energy* 367, 123382. <https://doi.org/10.1016/j.apenergy.2024.123382>.
- Sørensen, A.J., Fossen, T.I., Berge, S.P., 1997. Marine dynamic positioning systems. *Control Eng. Pract.* 5 (4), 481–486.
- Sørensen, A.J., 2013. *Marine Cybernetics: Modelling and Control of Marine Systems*. NTNU, Trondheim.
- Sung, I., Zografakis, H., Nielsen, P., 2022. Multi-lateral ocean voyage optimization for cargo vessels as a decarbonization method. *Transport. Res. Transport Environ.* 110, 103407. <https://doi.org/10.1016/j.trd.2022.103407>.
- United Nations Conference on Trade and Development, 2023. World investment report 2023: investing in sustainable energy for all. Retrieved from. <https://unctad.org/system/files/official-document/wir2023en.pdf>.
- Vergara, D., Alexandersson, M., Lang, X., Mao, W., 2023. A machine learning based Bayesian decision support system for efficient navigation of double-ended ferries. *J. Ocean Eng. Sci.* <https://doi.org/10.1016/j.joes.2023.11.002>.
- Wang, H., Mao, W., Eriksson, L., 2017. Benchmark study of five optimization algorithms for weather routing. *Proceedings of the ASME 2017 36th International Conference on Ocean, Offshore and Arctic Engineering*. Volume 7B: Ocean Engineering. ASME, Trondheim, Norway. <https://doi.org/10.1115/OMAE2017-61022>. June 25–30, 2017. V07BT06A023.
- Wang, H., Mao, W., Eriksson, L., 2019. A three-dimensional Dijkstra's algorithm for multi-objective ship voyage optimization. *Ocean Eng.* 186, 106131. <https://doi.org/10.1016/j.oceaneng.2019.106131>.
- Wang, H., 2020. *Voyage Optimization Algorithms for Ship Safety and energy-efficiency*.
- Wang, H., Lang, X., Mao, W., 2021. Voyage optimization combining genetic algorithm and dynamic programming for fuel/emissions reduction. *Transport. Res. Transport Environ.* <https://doi.org/10.1016/j.trd.2020.102670>.
- Wang, K., Li, J., Huang, L., Ma, R., Jiang, X., Yuan, Y., Mweru, N.A., Negenborn, R.R., Sun, P., Yan, X., 2020. A novel method for joint optimization of the sailing route and speed considering multiple environmental factors for more energy efficient shipping. *Ocean Eng.* 216, 107591. <https://doi.org/10.1016/j.oceaneng.2020.107591>.
- Wang, K., Yan, X., Yuan, Y., Jiang, X., Lodewijks, G., Negenborn, R.R., 2017. Study on route division for ship energy efficiency optimization based on big environment data. In: *Proceedings of the 4th International Conference on Transportation Information and Safety (ICTIS 2017)*, pp. 111–116. <https://doi.org/10.1109/ICTIS.2017.8047752>.
- Wang, K., Yan, X.P., Yuan, Y.P., Jiang, X.L., Lin, X., Negenborn, R.R., 2018. Dynamic optimization of ship energy efficiency considering time-varying environmental factors. *Transport. Res. Transport Environ.* 62, 685–698. <https://doi.org/10.1016/j.trd.2018.04.005>.
- Wu, W.-M., 2020. The optimal speed in container shipping: theory and empirical evidence. *Transport. Res. E Logist. Transport. Rev.* 136, 101903. <https://doi.org/10.1016/j.tre.2020.101903>.
- Wei, Z., Zhao, L., Zhang, X., Lv, W., 2022. Jointly optimizing ocean shipping routes and sailing speed while considering involuntary and voluntary speed loss. *Ocean Eng.* 245, 110460. <https://doi.org/10.1016/j.oceaneng.2021.110460>.
- Wen, Y., Sui, Z., Zhou, C., Xiao, C., Chen, Q., Han, D., Zhang, Y., 2019. Automatic ship route design between two ports: a data-driven method. *Appl. Ocean Res.* 88, 102049. <https://doi.org/10.1016/j.apor.2019.102049>.
- Xie, X., Sun, B., Li, X., Zhao, Y., Chen, Y., 2023. Joint optimization of ship speed and trim based on machine learning method under consideration of load. *Ocean Eng.* 287, 115917. <https://doi.org/10.1016/j.oceaneng.2023.115917>.
- Yan, R., Wang, S., Du, Y., 2020. Development of a two-stage ship fuel consumption prediction and reduction model for a dry bulk ship. *Transport. Res. E Logist. Transport. Rev.* 138, 101930. <https://doi.org/10.1016/j.tre.2020.101930>.
- Yan, R., Yang, D., Wang, T.Y., Mo, H.Y., Wang, S.A., 2024. Improving ship energy efficiency: models, methods, and applications. *Appl. Energy* 368, 123132. <https://doi.org/10.1016/j.apenergy.2024.123132>.
- Yan, Z., Xiao, Y., Cheng, L., He, R., Ruan, X., Zhou, X., Li, M., Bin, R., 2020. Exploring AIS data for intelligent maritime routes extraction. *Appl. Ocean Res.* 99, 102271. <https://doi.org/10.1016/j.apor.2020.102271>.
- Yeh, W.-C., Tan, S.-Y., 2021. Simplified swarm optimization for the heterogeneous fleet vehicle routing problem with time-varying continuous speed function. *Electronics* 10 (15), 1775.
- Yu, Y., Zhang, H., Mu, Z., Li, Y., Sun, Y., Liu, J., 2024. Trim and Engine Power Joint Optimization of a Ship Based on Minimum Energy Consumption over a Whole Voyage.
- Zaccone, R., Ottaviani, E., Figari, M., Altosole, M., 2018. Ship voyage optimization for safe and energy-efficient navigation: a dynamic programming approach. *Ocean Eng.* 153, 215–224. <https://doi.org/10.1016/j.oceaneng.2018.01.100>.
- Zhang, D., Zhang, Y., Zhang, C., 2021. Data mining approach for automatic ship-route design for coastal seas using AIS trajectory clustering analysis. *Ocean Eng.* 230, 109535. <https://doi.org/10.1016/j.oceaneng.2021.109535>.
- Zhang, M., Tsoulakos, N., Kujala, P., Hirdaris, S., 2024. A deep learning method for the prediction of ship fuel consumption in real operational conditions. *Eng. Appl. Artif. Intell.* 130, 107425. <https://doi.org/10.1016/j.engappai.2023.107425>.
- Zhang, S., Shi, G., Liu, Z., Zhao, Z., Wu, Z., 2018. Data-driven based automatic maritime routing from massive AIS trajectories in the face of disparity. *Ocean Eng.* 159, 56–65. <https://doi.org/10.1016/j.oceaneng.2018.02.060>.
- Zhang, Y., Ma, Y., Liu, J., 2024. Ship trajectory segmentation and semisupervised clustering via geospatial background knowledge. *Ocean Eng.* 304, 117872. <https://doi.org/10.1016/j.oceaneng.2024.117872>.
- Zheng, J.Q., Zhang, H.R., Yin, L., Liang, Y.T., Wang, B.H., Li, Z.B., Song, X., Zhang, Y., 2019. A voyage with minimal fuel consumption for cruise ships. *J. Clean. Prod.* 215, 144–153. <https://doi.org/10.1016/j.jclepro.2019.01.032>.